The Thesis Committee for Germán Chaves

Certifies that this is the approved version of the following Thesis:

Effect of Sub-seismic Reservoir Heterogeneity on CO_2 Plume Migration, Onshore Gulf of Mexico (Texas, USA)

APPROVED BY

SUPERVISING COMMITTEE:

Committee

Dr. Alex Bump, Supervisor

Dr. Seyyed Hosseini, Co-Supervisor

Dr. Carlos Uroza, Reader

Effect of Sub-seismic Reservoir Heterogeneity on CO_2 Plume Migration, Onshore Gulf of Mexico (Texas, USA)

by

Germán Chaves

Thesis

Presented to the Faculty of the Graduate School of

The University of Texas at Austin

In Partial Fulfilment of the Requirements

for the Degree of

Master of Science in Energy and Earth Resources

The University of Texas at Austin

December 2024

Dedication

I would like to dedicate this job to my entire family, who give me the strength and energy to wake up every day and strive to be a better person.

To my wife Claudia, who gave me the courage I needed when I decided to embrace this adventure; she helped me follow my dreams and gave me all the love and support I needed, always standing by my side during this time. To my mom, who is always watching over me from heaven; to my dad, for being a model of honesty and resilience throughout my life; to my brother, for giving me unconditional love and positive energy every single day; and to my sisters, who have always shared their wise words and unwavering support. And last but not least, to Maya and Achira, because they have made my life brighter. Without you, this journey would not have been the same.

Acknowledgements

I would like to express my deepest gratitude to my advisors, Dr. Alex Bump and Dr. Seyyed Hosseini, for their invaluable guidance throughout this journey.

My heartfelt thanks also go to Dr. David Hoffman, Dr. Carlos Uroza, and Dr. David Carr and Previna Arumugan for their crucial assistance with the geomodelling work, you guys did an amazing job in such a short time.

I am also truly grateful to all the GCCC team for their unwavering support during this time, you all showed me a new world and industry that opened my eyes.

I also would like to thanks to the Jackson School of Geoscience and the director of the EER program Dr. Fred Beach for all the support and advise during my studies.

Finally, I extend my appreciation to my friends and all those who contributed with their inputs and shared meaningful conversations, enriching this study in countless ways.

Abstract

Effect of Sub-seismic Reservoir Heterogeneity on CO_2 Plume Migration, Onshore Gulf of Mexico

Germán Chaves, MSEER

The University of Texas at Austin, 2024

Supervisor: Alexander Bump, Seyyed Hosseini

This study examines the impact of sub-seismic faults and channels on CO_2 plume behavior in the Lower Miocene formation in an onshore area of the Texas Gulf of Mexico. This geological formation is characterized by heterogeneous reservoirs with an important amount of unconsolidated fluvial sandstones, where sub-seismic faults and channels are challenging to identify using conventional seismic methods. The research focuses on potential unintended lateral migration of CO_2 and changes to the area of review (AoR) size beyond the leasing area in carbon capture and storage (CCS) projects.

A methodology was developed to characterize sub-seismic faults and channels by integrating seismic data, literature correlations, and well log analysis. Fault seal capacity was estimated using a combination of shale gouge ratio (SGR) and transmissibility multiplier approaches, yielding fault transmissibility values higher than 0.1 as a realistic value for sub-seismic faults. Additionally, a workflow for generating capillary pressure and relative permeability curves was established, integrating literature data and well-known correlations. This workflow enables reservoir engineers to include these curves in the simulation even in data-scarce regions.

Experimental static models were built using available geological information, including 2D/3D seismic amplitude extractions, well log correlations, and core data integration. These were

followed by dynamic simulations incorporating these sub-seismic features in synthetic, single-unit, and full-field models. Sensitivity analyses on geological uncertainties and sub-seismic fault characteristics revealed that sub-seismic faults with transmissibility values higher than 0.1 have minimal impact on the AoR size and shape. CO_2 migration was confined to high-permeability injection zones, while pressure dissipation occurred throughout the model, with low-permeability zones acting as pressure buffers.

The full-field models validated these findings under realistic operational constraints, demonstrating that sub-seismic features do not significantly influence unintended CO_2 migration or pressure buildup in most scenarios. Additionally, low-permeability zones were found to act as barriers to CO_2 flow and as pressure dissipation reservoir units, reducing AoR size and shape.

These findings suggest that operators should prioritize seismic-scale feature characterization and consider heterogeneous geological settings without the need of regional seals for CO_2 injection. Proper boundary definitions are critical for optimizing AoR size, minimizing costs, and enabling CCS projects in areas previously considered as unsuitable. - This study highlights the potential of composite confinement systems concept in enabling effective CO_2 storage in complex geological environments.

Table of Contents

LIST OF TABLES

LIST OF FIGURES

1. CHAPTER I

1.1.INTRODUCTION

Reducing global greenhouse gas emissions, particularly carbon dioxide (CO_2), is a critical global concern. In the US, approximately 1,600 million metric tons of annual CO_2 emissions (32% of the total yearly CO_2 emissions in the US), coming mainly from activities such as burning fossil fuels for electricity, transportation, and industrial processes were classified as easy to capture sources of CO_2 (GAO, 2022), being those emissions, the focus of the first CO_2 reduction projects currently developed in the US. The constant increase of CO_2 concentration in the atmosphere observed during the last decades has been considered as one of the factors affecting climate change. This surge in CO_2, a major contributor to global warming, correlates with increased energy consumption, aiding economic development but intensifying environmental challenges (European Environment Agency, 2014). Acknowledging this, many countries, as per UN agreements (UN, 2015) are committed to reducing CO_2 emissions in the following years.

Different alternatives are being evaluated and implemented worldwide to reduce CO_2 emissions including but not limited to: i) electrification of transportation to reduce fossil fuel consumption, ii) replacing fossil fuel electricity generation by renewable energy use such as solar, wind, hydrogen, and geothermal, iii) permanently storage of CO_2 underground using carbon capture and storage technology, among others. Carbon Capture and Storage (CCS) technology emerges as a potential contributor to CO_2 emissions reduction, capturing large amounts of CO_2 from industrial processes and storing it underground either in saline aquifers or depleted oil or gas reservoirs (GAO, 2022).

After 50 years of investigation and research, CCS has been demonstrated as an effective way to safely store CO_2 for geological time periods. A wide spread of commercial CCS deployment in the US is ongoing, mostly due to government incentives that would allow operators to capture and store CO_2 safely and economically, keeping worldwide commitments to reduce CO_2 emissions. While some global projects are underway, the current capture capacity remains modest (50.5 Mtons/year worldwide and 25.9Mton/year in the US for 2024), representing less

than 2% of total global emissions (37 Gt of CO_2/year) which implies that an increase in the order of Gigatons in capture is required to achieve the UN agreements (IEA, 2023).

The Onshore Gulf of Mexico Basin (GOM) has become a focal point for CCS initiatives in the US due to its established geology, regulatory clarity, and proximity to large CO_2 sources like power plants and industrial facilities. Collaborative efforts between the US government, research institutions, and operators aim to establish a robust CCS industry, and address common concerns and challenges related to underground CO_2 storage.

For carbon capture and storage projects being developed in the GOM, Operators' business incentive is to fill their current leases with CO_2, right up to the lease lines. This is a reasonable starting point, and a good business plan that maximizes the value of the lease. Initial scoping of CO_2 projects starts with isotropic models of radial plume growth around the injector (s) assuming a simple geology and homogeneous petrophysical model for the injection zone (s). As the injection prospect is developed, models to represent fluid flow get more sophisticated, and additional geology information is considered. Small features such as heterogeneities (channels) and sub-seismic faults can be found in the models and would impact the fluid flow behavior of the CO_2 plume.

1.2.STATEMENT OF THE PROBLEM

Onshore Gulf of Mexico area has a complicated geology, and developing CCS projects in that area is not that simple. Most of the surface area onshore Texas is characterized by multiple oil and gas fields, agricultural and industrial uses. At the same time, subsurface is far from being homogeneous, on the contrary, is considered for being heterogeneous, with the presence of multiple fluvial channel systems, big quantity of strike-parallel faults with high throw and multiple salt diapirs (Figure 1). Considering surface and sub-surface limitations, the geology characterization, location definition and CO_2 migration within leasing areas has become of great relevance for operators during CCS project development. Geological features mentioned before can be easily identified by seismic interpretation and be considered during site characterization and CO_2 fluid flow predictions, but, sub-seismic features, such as, sub-seismic faults and

channels could also be present in these geological environments and can´t be easily identified through conventional seismic methods. So, the possible unintended lateral migration of CO_2 beyond the leasing area due to sub-seismic faults and channels is the main problem to be addressed in this study.

Most of the time, CO_2 and pressure plume don't not grow radially due to heterogeneities in the injection zone mentioned before. Understanding the geological uncertainties and possible deviations of radial CO_2 plume growth outside leasing area due to heterogenous features such as sub-seismic faults and channels is the main concern in this research.

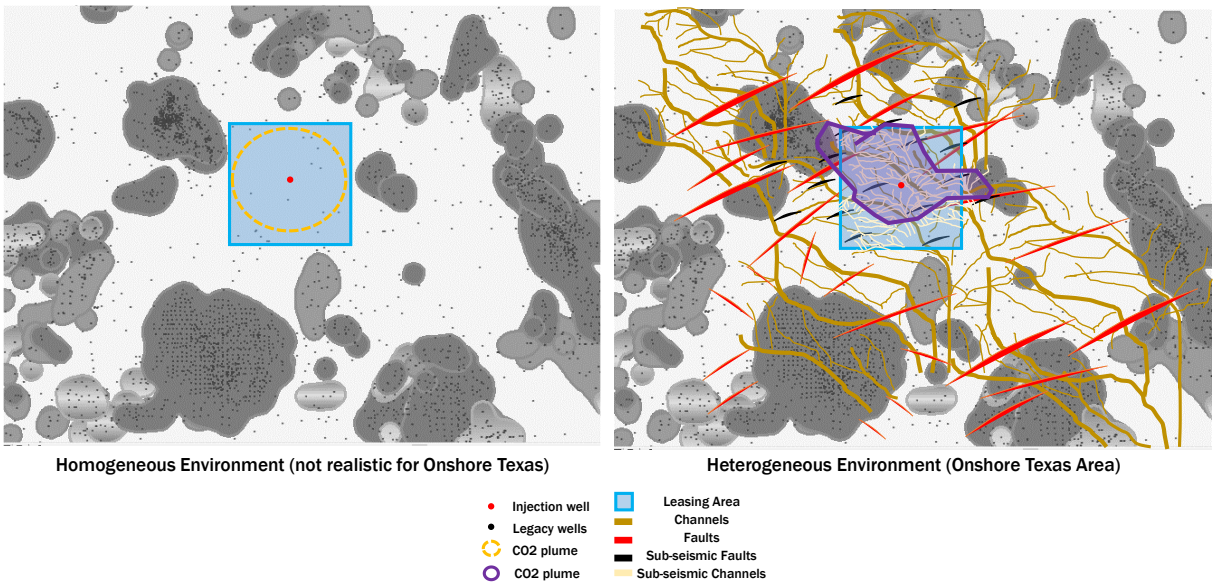

Figure 1. CO_2 plume shape due to Heterogeneous environments – CO_2 outside the leasing area

This study aims to investigate the CO_2 plume migration in complex environments that include channelized reservoirs and strike-parallel faults in the Lower Miocene formation onshore of Texas at a depth of around 5,000 ft. This research includes analytical and numerical modeling to investigate the fluid flow behavior of the CO_2 plume, using a real project as the starting point to generate a range of geologic models that include varying degrees of anisotropy.

1.3.OBJECTIVES

For this study, I aim to investigate the impact of features such as reservoir heterogeneities (channels) and sub-seismic faults in the CO_2 plume behavior using an example of a real site located onshore GOM where channelized reservoir and faults are found.

Understanding plume migration through complex environments, as the one described above is crucial because it will help operators to comprehend:

- Risk of lateral migration of CO_2 beyond lease boundaries that would put the operator out of compliance and at risk of fine or lawsuit.
- Risk of CO_2 contacting elements that might allow vertical migration. This unintended migration could imply additional costs for remediation operations required to contain the CO_2 migration in the case of a leakage (i.e., through a leaky well).
- Risk of loss of injectivity in the injection wellbores due to pressure buildup, which could cause reduction of CO_2 store capacity and impact in the economics of the project.
- Risk of lost revenue due to underutilizing the reservoir if injection has to be shut down to keep plume growth inside the lease lines.
- Risk of unanticipated pressure propagation that causes area of review (AoR) to be different to what was predicted or could cause pressuring up of neighboring fields. This could require an extensive integrity review or remediation of many old wells.

1.4.RELEVANCE

Operators are currently facing different challenges to make CO_2 capture and sequestration commercially viable; with reduction of cost of capture and storage as one of the main concerns. To reduce the cost of CCS, operators are proposing injection close to the main CO_2 sources, which implies injecting in very complex geological environments along the onshore Gulf of Mexico basin. There are currently many commercial projects in development on the Gulf Coast area as illustrated in Figure 2. Those projects are being developed in heterogeneous geology and with oddly-shaped leases. Understanding the risks and consequences associated with

unintended lateral migration outside the leasing area in these heterogeneous environments are of main importance for operators.

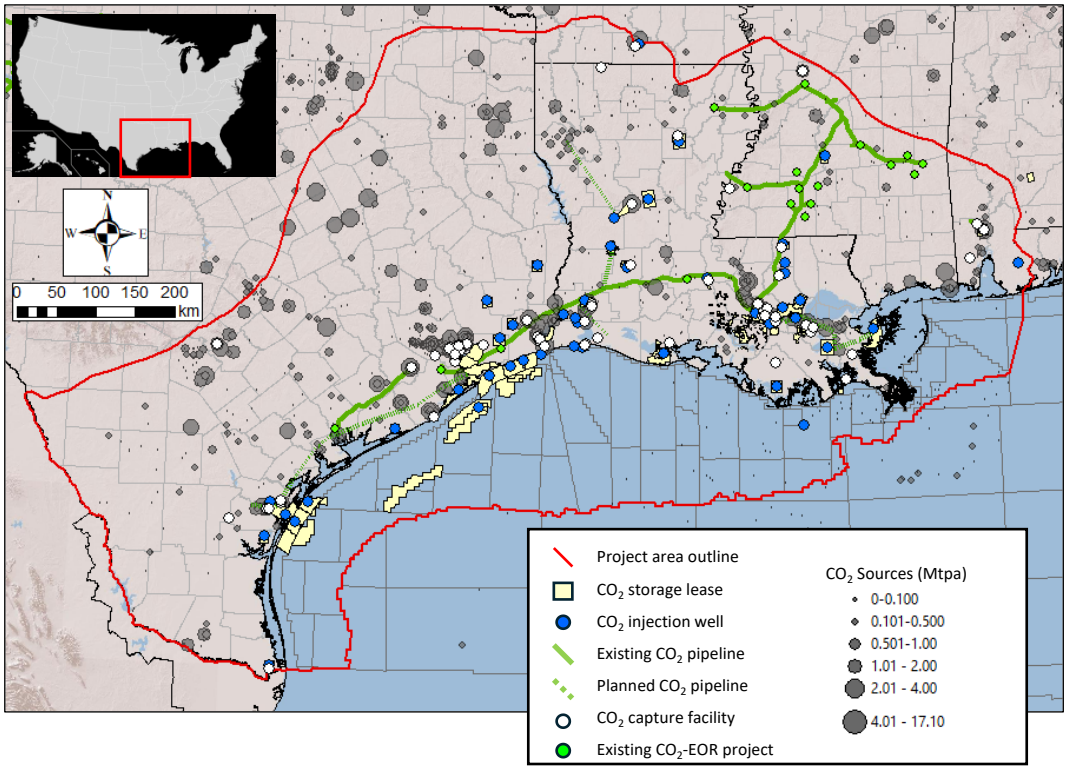

Figure 2. Gulf of Mexico – CO_2 sources, pipelines, CO_2 injection projects and leasing areas (Provided by Dr. Alex Bump, GCCC, 2023)

Operators require clear and trustworthy insights to the main concerns related to the unintended CO_2 migration in the projects that are developing in the onshore Gulf of Mexico basin to advance with commercial deployment of the CCS in this region.

Results obtained from this study will help the operators to identify what parameters are relevant for their projects and what information should be acquired before injection starts, to have a better characterization of the area of interest and reduce risks associated with the unintended CO_2 migration outside the leasing area. Identifying cases where unintended migration or unintended pressure build up are most likely and determining the associated risks and mitigation strategies to avoid those behaviors is of main importance for the technical and economic viability of any CCS project.

1.5.CHAPTER ORGANIZATION

The Chapters below are organized as follows: Chapter II will give a background of previous studies related to heterogeneous reservoirs and faults characterization in other Gulf of Mexico sites that will help to characterize the area of interest for this study. Chapter III will present the methodology used in this research to solve the proposed problem. Chapter IV will present the main analysis and results of the study. Chapter V is dedicated to the discussion of the main insights found with this research and Chapter VI will enumerate the main conclusions obtained during this work.

2. CHAPTER II

2.1.RESEARCH BACKGROUND

This chapter will provide a context to understand the work that will be presented during this study. It includes an overview of the reservoir characterization in the GOM area, previous studies on reservoir characterization for carbon capture and storage projects, not only in the onshore Gulf of Mexico but also in other basins and will also include some key concepts that will be used during this research. The objective of this review is to identify previous investigations that could help to characterize the main features that will be included in this research. Identifying methods to characterize channelized reservoirs, faults, and sub-seismic faults and channels that will help us to build a more realistic CO_2 plume model are the focus of this review.

2.1.1 Reservoir characterization of the Gulf of Mexico area in the USA

The Gulf of Mexico is situated along a passive margin on the southern U.S. coast. It has a geologic history rooted in the breakup of Pangea around 200 million years ago during the Late Triassic to Early Jurassic periods. As tectonic rifting opened the Gulf, extensive evaporite

deposits, including the Louann Salt Formation, accumulated within the rift basin. These Jurassic salt layers now underlie the Gulf's sedimentary sequences and are integral to the region's structure, with salt movement creating ideal conditions for hydrocarbon traps (Salvador, A., 1991). By the mid-Jurassic period, active extension gave way to oceanic spreading, transforming the Gulf into a passive margin characterized by carbonate platform development, including the Smackover Formation, which features extensive limestone and dolomite deposits (Galloway et al., 2000). In the Cenozoic era, large rivers, especially Red River, Rio Grande, and Mississippi River fluvial axis, delivered substantial sediment loads, forming thick sedimentary layers and deltas. These complex interactions of tectonics, sedimentation, and salt dynamics have crafted a stratigraphy that remains one of the most complex systems in the Gulf of Mexico area (Galloway et al., 2000).

The geological formations of interest for this study are injection zones of Miocene and Oligocene age. They originated by a massive sediment influx primarily dominated by the paleo Red River fluvial axis in the onshore of Texas (Galloway et al., 2000). Those fluvial deposits tend to have a flow direction perpendicular to the coastline, generating an anisotropic and heterogeneous property distribution along the reservoir (channels).

Coast-parallel regional faults create a different anisotropy at 90° degrees to the first. These normal faults in the W-E direction parallel to the coastline are easily identified in 2D and 3D seismic. They are the result of the gravitational collapse/spreading of the passive margin or accommodating differential subsidence around salt diapirs. In Figure 3, general representation of the depositional systems in the GOM Lower Miocene Paleogeography deposits is presented, with a representation of the main flow channels direction and faults presence. The area of interest for this study is highlighted in the purple box. Figure 4 presents a cross section of the lower Miocene formation onshore and offshore of Texas area, where the heterogeneous deposits of the lower Miocene formation are identified.

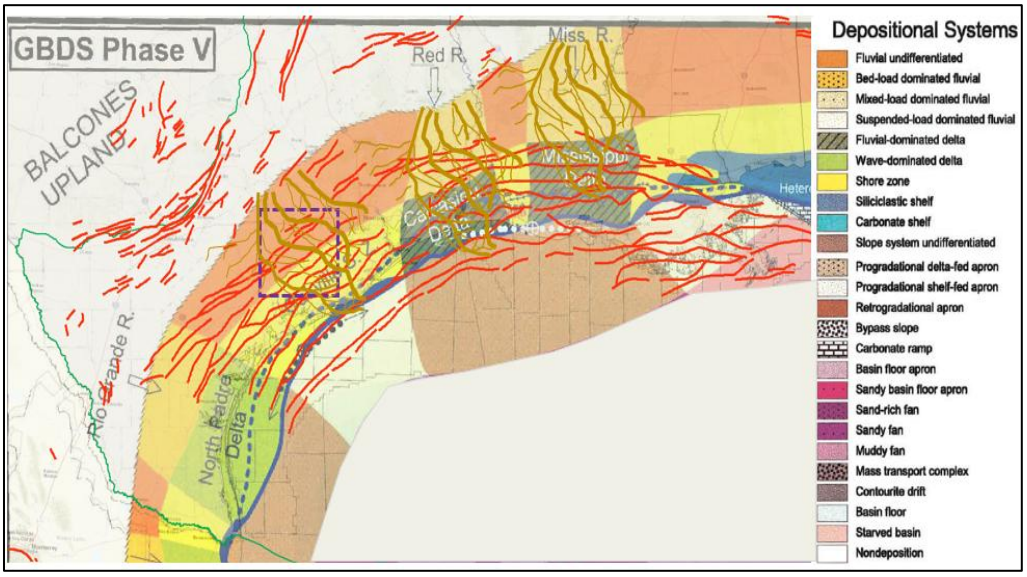

Figure 3. Paleogeography of the Lower Miocene Formation, adapted map from (Galloway et al., 2000)

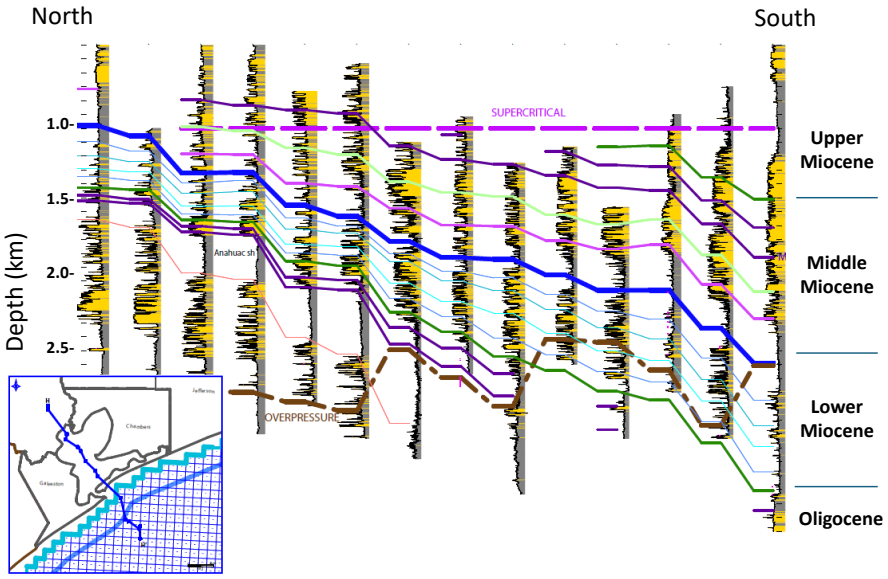

Figure 4. Well correlation in Miocene formation – heterogeneous geology in the Gulf of Mexico (Provided by Dr. Alex Bump, GCCC, 2023)

The accumulation of these sediments, along with salt tectonics, generated key geologic features like growth faults and salt domes, that generated good reservoirs and seals for hydrocarbon reservoirs. During the last century, several oil, gas and water disposal wells have been drilled to produce the resources trapped in the sub-surface of the GOM area (Figure 5). The aggressive drilling of these kind of wells leaves little space for CO_2 injection in the surface and subsurface.

Operators want to be away from the legacy wells to reduce risk associated to CO_2 leakage, and trying to find those areas where a low number of legacy wells are present is a constraint to identifying possible CCS project locations.

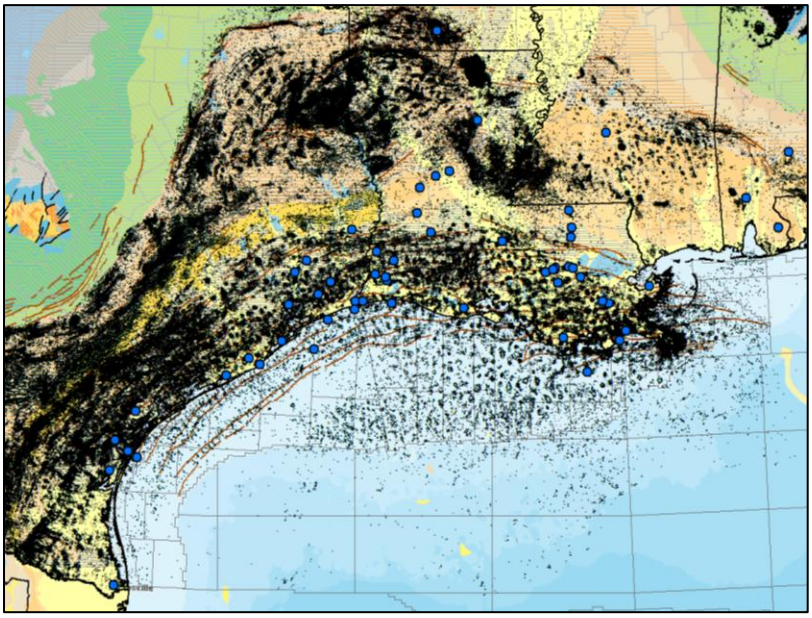

Figure 5. Legacy wells in black (oil, gas and disposal wells) –Gulf of Mexico area (Provided by Dr. Alex Bump, GCCC, 2023)

With the aim to identify areas suitable for CCS, some previous studies have demonstrated the good potential for CO_2 storage of the Miocene and Oligocene saline aquifers in the Onshore GOM (Bump., 2023; Zulqarnain., 2023; Bruno., 2014; Treviño and Meckel., 2017). Operators have used that information to identify and propose the best areas for CCS projects.

Currently there are many commercial projects in development on the Gulf Coast as illustrated in Figure 2. Those projects are being developed in heterogeneous geology and with oddly-shaped leases. Operators are locating the projects close to the main CO_2 sources and existing pipeline infrastructure. Understanding the risks and consequences associated with unintended lateral migration outside the leasing area in these heterogeneous environments are of main importance for operators.

2.1.2 Reservoir modeling

Static and dynamic reservoir modeling of CCS projects is of main importance for Class VI CO_2 injection permits. Modeling reservoirs for CCS is not the same as modeling reservoirs for conventional oil and gas project; Understanding the best approaches used for modeling this kind of reservoirs was achieved through literature review and analysis of previous studies.

Potential CO_2 injection formations in the GOM are characterized by fluvial-dominated deposits that created heterogeneous and anisotropic environments with significant changes in reservoir properties, such as porosity and permeability within the Miocene and Oligocene aquifer formations. Several studies have investigated the effect of heterogeneous facies in the CO_2 plume growth. In those studies, the importance of a good geologic characterization of the facies is always mentioned due to the considerable implications of heterogeneities in flow behavior.

According to (Hosseini et al., 2013), modeling heterogeneous facies to build a fairly real static model is valuable, and how you model it would have a big impact on the storage capacity of the injection zone and the size of the CO_2 plume in the area of interest. In his studies, this is achieved by using an object modeling approach, using seismic interpretation, well log data, core data and any other information available to define depositional facies and assign properties to each one of them and generate the most realistic model.

Modeling sub-seismic features such channels is also required for this study. Some of these features can be mappable with well data or core information, meanwhile, others can't be easily identified but could play a big role in the CCS project. According to Krishnamurthy et al., (2022) study, sub-seismic heterogeneities can change the volume of the reservoir contacted by CO_2 and the trapping of the phase in the contacted regions. Some sand tank studies have demonstrated how small geometry changes and grain size contrasts will play a big role in CO_2 plume growth. As an example, (Ni et al., 2023) study showed that almost 80% of the trapped CO_2 could be caused by sub-seismic heterogeneities that are not easily identified. Gathering data related to the depositional setting and depositional facies in the area of interest is relevant and will give a better understanding of the flow behavior.

Some studies (Gillespie et al., 2018; Maerten et al., 2006; Olson et al., 2009; Yaghoubi, 2019) have investigated different methods to model sub-seismic faults, such as geomechanical models, finite discrete elements models, heuristic mechanical models, discrete fracture network models, among others. Due to the complexity and unpredictable location of sub-seismic faults in a reservoir, a stochastic approach can be implemented using discrete fracture network modeling, where the sub-seismic faults would be placed independently according to the stochastic method. This method has been used constantly before due to flexibility and computational advantages, for that reason will be investigated in detail and its applicability for this project will be evaluated.

Faults are common in the GOM area and many of them are known to seal hydrocarbon accumulations. Fault modeling has been studied for decades due to its sealing capacity, meanwhile, their effect on CO_2 migration is not well known. Several authors have investigated different methods to model faults and faults sealing capacity and properly include them in geologic static models. Majority of fault sealing analysis are focused in fault zone architecture and seal analysis (Pei et al., 2015). Methods such as shale gauge ratio, clay smear potential, shale smear potential and scaled share gauge ratio have been used in different studies, being the shale gauge ratio the most used (Clarke et al., 2005; Miocic et al., 2019; Nicol et al., 2017; Snippe et al., n.d.). Using the fault information available for this specific site project, the best method to model faults were evaluated and the best approach to represent these faults in the dynamic fluid flow model were determined.

After a representative static model construction is obtained, dynamic fluid flow simulation of the CO_2 flow behavior should be performed using any commercial simulators such as Petrel or CMG. (Alfi & Hosseini, 2016; Delshad et al., 2013; Hosseini et al., 2013) have used programs like the ones mentioned before to perform the fluid flow evaluation. Several aspects have to be considered during this stage and will be analyzed during the study. Evaluation of the software was performed in order to identify the optimal one to use in this project. The expertise of the BEG and UT researchers was very useful in performing the dynamic fluid flow approach to this problem.

2.1.3 Saturation functions

One of the most important parameters during dynamic modeling of CO_2 storage in saline aquifers are relative permeability (kr) and capillary pressure (Pc) curves. Adequate curves are critical for fluid flow behavior and storage capacity of injection zone. These curves are water saturation-dependent and their values could be obtained either by core lab tests, analog data, or known correlations.

Most of the time, core and core plugs are not available for CCS projects due to the lack of stratigraphic wells in the area of interest, or economic limitations that does not allow core programs in new stratigraphic wells. Frequently, legacy wells close to the area of interest were drilled decades ago and were abandoned after running basic well logs and lack of oil or gas accumulations were interpreted. If no cores were obtained during the drilling phase, no lab tests to obtain relative permeability and capillary pressure curves are possible to obtain.

2.1.4 Composite confinement system definition

In most of the areas proposed for CCS projects, there is a lack of a regional seals, so operators are looking for new storage concepts for their projects. One of these is the composite confinement system concept proposed by (Bump, 2023), which states that “a composite confinement system of individually imperfect barriers can create highly effective confinement”. As a reference, Figure 6 presents this concept:

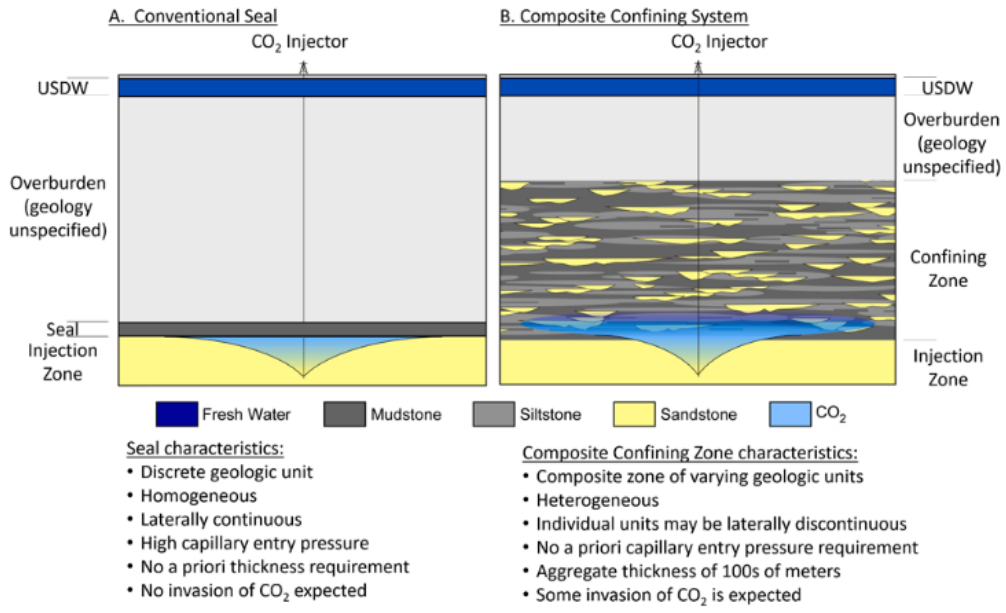

Figure 6. Composite confinement system concept (Bump, 2023)

This novel concept could increase the storage capacity in zones where no regional seal is observed and in injection zones not considered before as a reservoir for storage that will constrain the CO_2 to the injection zone. The effectiveness of the composite confinement system concept will be evaluated during this study in a full-field model.

2.1.5. Area of review definition

Operators want to be away from the legacy wells and possible leakage paths, for that reason, the AoR concept should be introduced. Main results in this study will be presented in terms of CO_2 saturation, pressure front, and Area of Review (AoR). Before presenting the results obtained in the static and dynamic simulation models, it is important to understand this concept.

U.S. Environmental Protection Agency (EPA) requires operators to protect the underground source of drinking water (USDWs) from the CO_2 migration. Operators have to guarantee that CO_2 injected for CCS projects won't reach the USDWs through any leakage point such as producing/legacy wells, faults, fractures, cap rock breaks or pinch-out or dip layers, among others.

In order to protect the USDWs, EPA defines the edge of the computed AoR as the region at which the pressure build-up at any time is able to lift the formation water of the injection zone to the base of the USDW through open conduits. This means, that it is important to define the edge of the AoR and this edge will be determined by the minimum pressure required by the water present in the injection zone to reach the USDW which are located at shallower formations. Some methods have been developed by researchers (Nicot et al., 2009) and operators in order to define the AoR adequately. Reservoir dynamic modeling can be used to define the AoR for the Class VI permits and will be used for this study.

3. CHAPTER III

This chapter includes the methodology used to conduct this study. Initially, characterization of heterogeneity features such as sub-seismic and channels in the area of interest are presented. Then, a first approach of modeling the CO_2 plume and pressure for simple but realistic models using the information previously extracted is performed. Finally, the insights were applied into a full field development project. Uncertainties related to the sub-seismic faults and channels characteristics and the implication of those features on the CO_2 plume shape and area of review (AoR) are presented.

3.1. DATA AND METHODOLOGY

The methodology used for this study is composed of four main sections, that will allow to understand and evaluate the effect of sub-seismic reservoir heterogeneities in the CO_2 fluid flow behavior. The first section is related to characterization of heterogeneity features such as sub-seismic faults and channels which are critical for this study. Second section involves building a simple model to understand the impact of reservoir heterogeneities in CO_2 fluid flow behavior. Third section will consist in building realistic but flexible models in the area of interest to experiment with. Fourth section will compile all the insights obtained in previous sections and consist in building a full field static and dynamic model using the available data from the

unnamed project and determine main uncertainties related to reservoir heterogeneities and the effect of them in the CO_2 plume and pressure front.

3.1.1. Reservoir Characterization

Large faults and channels, as well as, their reservoir characteristics have been well identified in earlier studies through 2D and 3D lines seismic interpretation, geologic characterization, and historical oil and gas drilling reports, but smaller heterogeneities such as faults and channels (sub-seismic size) are not easily identified due to the resolution limitations of the tools currently used in seismic acquisitions and interpretation.

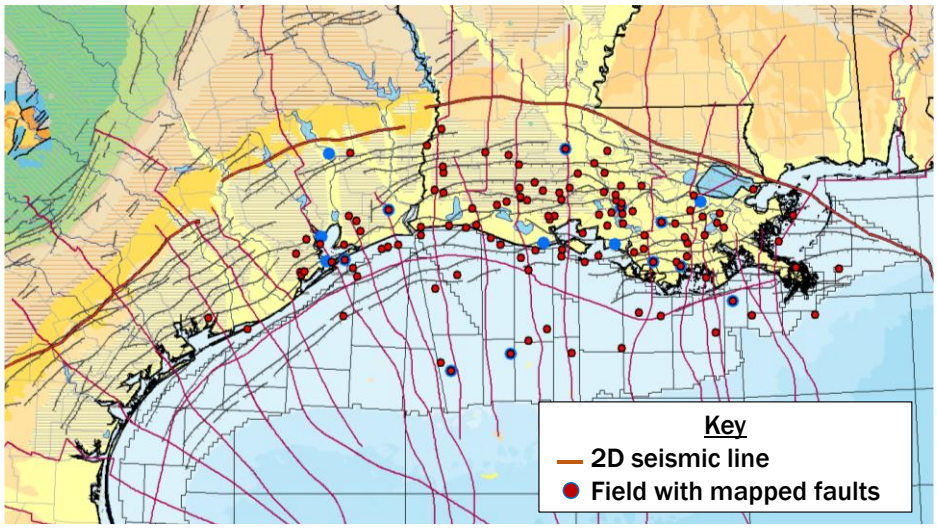

Figure 7. Gulf of Mexico – Schematic of information used for reservoir characterization (Provided by Dr. Alex Bump, GCCC, 2023)

For this study, more than 2,000 km of 2D seismic, 15 published field maps and two 3D seismic surveys were used to characterize seismic faults (Figure 7). This information, combined with more than 150 well logs with SP and Gr measurements and one new stratigraphic well with core and complete well-log data in the area of interest, are part of the database used during this research.

Additional research was conducted to obtain real site-based information such as porosity-permeability relationships and channels characteristics to fairly represent the geology of this site.

3.1.1.1 Channel's characterization

Information on channel geometries come mainly from two sources: local seismic amplitudes extractions and literature.

Facies (Channels) characterization including width, thickness, trends, and frequency is required. In some studies (Armstrong et al., 2014; Gibling, 2006; John S. Bridge2 And Robert S. Tye3, 2000; M. I. Olariu et al., 2019), information regarding these parameters for the Miocene formation in analog areas close to the area of interest were found. Further investigation was done to include the best parameters for channel characterization in our model and be able to build a representative static model.

Channel geometries (width, thickness, wavelength and amplitude) were taken from local seismic amplitude extractions provided by the BEG department (e.g., Figure 8), local published literature and global analogs.

Studies carried by authors such as (A. D. Reynolds, 1999; Armstrong et al., 2014; Gibling, 2006; John S. Bridge2 And Robert S. Tye3, 2000; Larue et al., 2023; Lowry & Jacobsen, 1993; C. Olariu & Bhattacharya, 2006; Reynolds, 2017) were also used to for channel characterization and help to determine empirical correlations between the width and thickness of several channel environments.

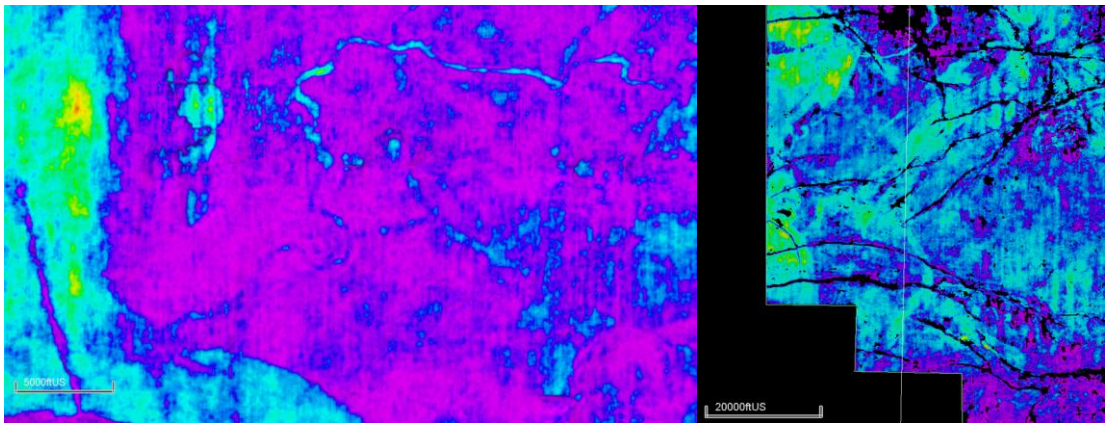

Figure 8. Amplitude extractions of the offshore GOM area (Provided by GCCC)

Correlations such as the one presented in Figure 9 was used to determine average thickness of the fluvial channels' sets that were previously characterized through amplitude extractions interpretation. Thickness values between 30-100 ft were obtained for set No. 1 and values of thickness lower than 30 ft were determined for the set No. 2 channels. This information was considered during the static models' generation.

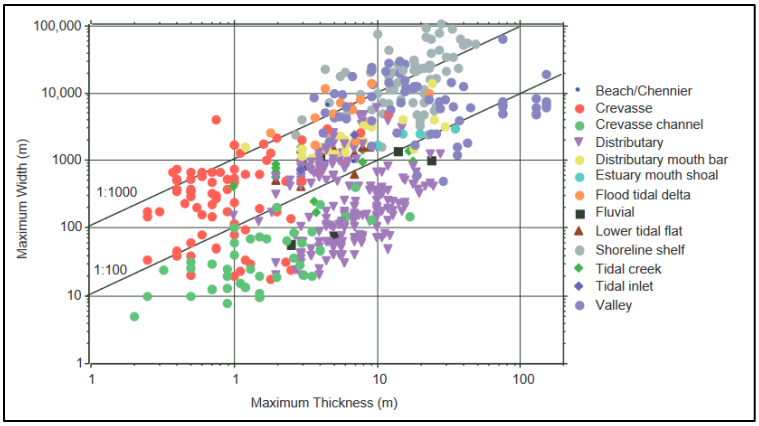

Figure 9. A log vs. log plot of width vs. thickness for different sand body types. Sand body types show clear clustering and only limited overlap of dimensions. Two lines recording thickness-to-width ratios of 1:100 and 1:1,000 are also presented (A. D. Reynolds, 1999)

Two different families of channels were identified in seismic amplitude extractions. Combination of these sets were taken as a reference in this study to build the initial models. The main parameters are presented in Table 1:

	Width (ft)			Wave Length (ft)			Amplitude (ft)		
	Low	Base	High	Low	Base	High	Low	Base	High
Set No. 1	1,500	2,500	4,000	12,500	15,000	17,000	10,000	12,500	15,000
Set No. 2	350	500	600	2,000	2,500	3,000	680	900	1,200

Table 1. Channel's geometrical characteristics used in first experimental models.

Petrophysical properties including porosity and permeability in the GOM area were obtained from literature (Fisher et al., 2018; Herve Jourde,1 Eric A. Flodin, Ati, 2002; Taylor & Pollard, 2000), and information provided by the operator. Studies performed by (Gutiérrez Paredes et al., 2018; Lowry & Jacobsen, 1993) in Miocene reservoirs in the southern Gulf of Mexico (Mexico) and in the Ferron Sandstone in east-central Utah respectively, were also used as a reference for petrophysical properties. Furthermore, more than 150 well logs of legacy wells were obtained in the area of interest and were used to determine petrophysical facies and calibrate the porosity and permeability values used in the models. Porosity and permeability values for each facies were populated in the probabilistic geological models based on all the previous information acquired.

3.1.1.2 Sub-seismic fault characterization

Sub-seismic faults direction is assumed to be sub-parallel to the regional coast-parallel regional faults but most of their characteristics are unknown. 2D/3D seismic lines and seismically visible faults obtained from literature were used to create distribution function and predict the sub-seismic faults characteristics. Predicted information was included in the models to evaluate the effect of those sub-seismic faults in the migration of CO_2 within the area of interest. Some of the main characteristics are:

Fault frequency and throw:

Fault throw and location data on more than 2,000 km of 2D seismic lines were compiled in this study. A methodology presented in previous studies (Pickering et al., 1996) to determine frequency of small faults using the observed data of frequency and throw of bigger faults that are observed in the 2D/3D seismic lines was used in this research. More than +200 data points related to faults' frequency and throw were obtained from 2D seismic lines from the GOM

onshore and offshore. Figure 10 presents the cumulative rank of frequency per km vs. throw relationship.

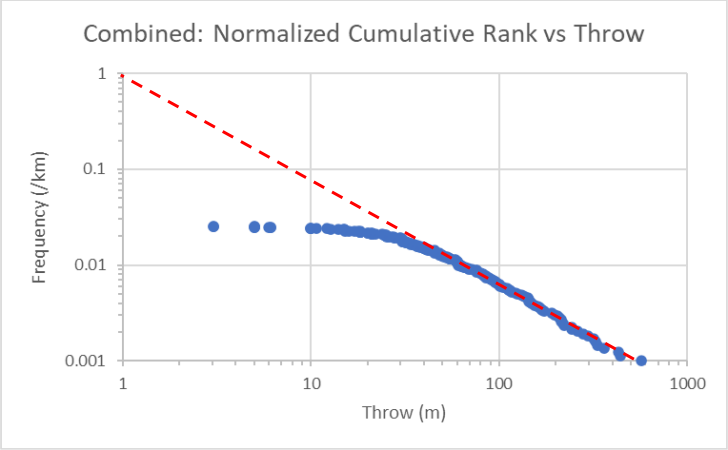

Figure 10. Normalized cumulative frequency vs. throw data points

Figure 10 shows that for throws below 30 meters fault frequency no longer follows a straight line in log-log space, which means that small faults are being under-sampled due to average 2D seismic vertical resolution. Additionally, from this figure, extrapolation can be done using the most likely linear tendency in the graph to determine the frequency of unseen or sub-seismic faults. As a result of this tendency, small throw faults (less than 30 meters throw) are not very frequent. According to this correlation, frequency of faults with 10 meters of throw is close to 0.1 faults per km, in other words, it could be around 1 fault per every 10 km.

Faults length and throw:

Data from published field maps and 2D/3D seismic lines from the onshore and offshore Gulf of Mexico in the Texas and Louisiana areas were analyzed. In this study, reports related to structural maps of oil and gas fields where faults length and throw can be identified were used (Figure 11).

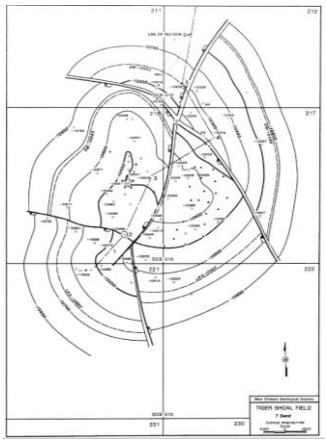

Figure 11. Example of a structural map from offshore Louisiana (Smith, 1988)

Faults' throw or displacement vs. length of the faults were obtained for several oil and gas fields. The collected data is presented in Figure 12, and from the data it can be inferred that most of the points are located between the lines of 1:10 and 1:100 relationship. In addition, faults with a throw lower than ± 30 meters (100 ft) can't be identified due to the average vertical resolution of the 2D/3D seismic (these are the sub-seismic faults) but it can be assumed that the relationship for those faults will follow the same trend and any point will be located between the two blue dotted lines.

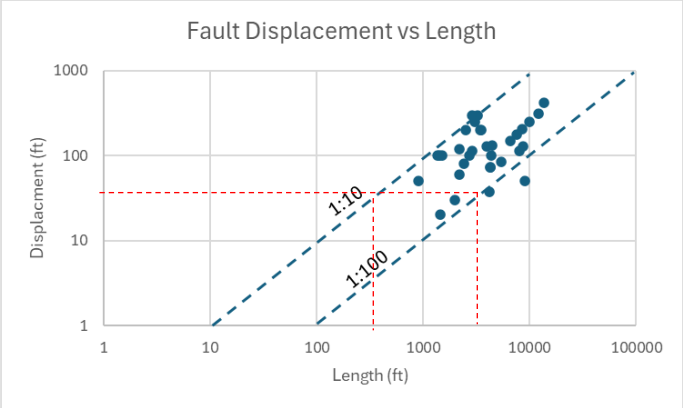

Figure 12. Fault displacement vs. Length (Provided by Dr. Alex Bump, GCCC, 2023)

Authors such as (Treviño et al., 2017) presented a similar correlation that confirmed the results obtained for the displacement vs. length relationships done during this study. According to the previous figure, sub-seismic faults that have less than 30 meters of throw can have lengths that

vary in the range of 1:10 and 1:100. As an example, a sub-seismic fault of 30 meters of throw could have a length up to 3,000 ft.

Fault seal capacity:

Fault seal capacity was addressed using the SGR concept in our area of interest. The area of interest is located in the onshore GOM at a depth of around 5,000 ft (Miocene formation) and to predict sealing capacity of faults with throws lower than 100 ft (30 meters) which are assumed to be the sub-seismic faults, the following workflow was performed:

1. Stratigraphic well log data in the area of interest (classified well name for confidentiality policies) was used to calculate the Vshale (Vsh) parameter.
2. Vsh coming from the stratigraphic well log data for the injection zone were used to calculate SGR for different fault throws.
3. A triangle diagram was generated in the proposed injection zone of the project. Figure 13 presents the created map.
4. Considering the sand thickness in the injection zone, and fault throws less than 100 ft (30 meters), SGR values between 2 and 45 were obtained for the injection sands. Is important to mention that SGR values above 20-25 are considered likely seals, so in this case sub-seismic faults would not to have a complete fault seal.

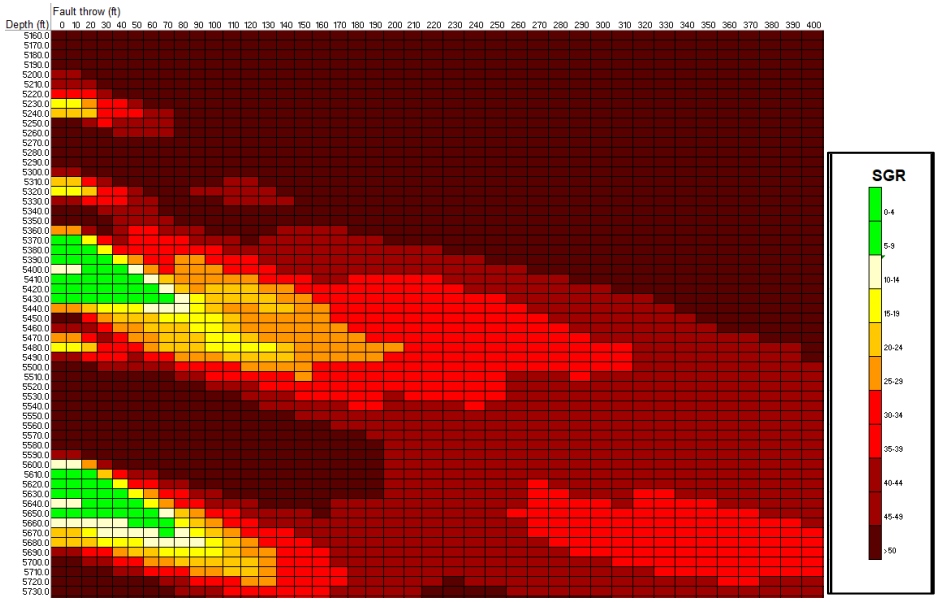

Figure 13. Shale Gauge Ratio vs. depth plot for a well in the area of interest

Shale gauge ratio is a good indicator of fault seal capacity in the injection zone but in order to include simulation faults in the dynamic model, properties such as fault permeability or transmissibility need to be calculated. Various studies have been carried out during the last decades to estimate permeability and/or transmissibility multipliers of faults using clay smear indices such as SGR. A methods developed by (Manzocchi et al., 1999) to estimate transmissibility multipliers for flow simulation models using the SGR as an input was used in this study. The following equations were used to calculate average transmissibility multipliers for the analyzed well within the area of interest:

$$T = \left[1 + t_f \times \frac{(2/k_f - 2/k_m)}{2L/k_f}\right]$$

Where:

T= Transmissibility multiplier

k_m=Matrix permeability

L=Grid cell size

t_f=Fault thickness, and is equivalent to $t_f = D/66,$ where D is the displacement or throw of the fault.

k_f=Fault Permeability and is calculated using the following equation:

$$\text{Log } k_f = 0.4 - 4 \times SGR - \frac{1}{4} log(D) \times (1 - SGR)^5$$

In the injection zone in the Miocene formation, transmissibility multipliers between 0.15 and 0.7 were calculated for faults with a throw less than 100 ft (30 meters), with an average value of 0.2.

3.1.1.3 Sub-seismic Fault characterization results

It is important to summarize the main results of sub-seismic faults characteristics obtained from the methods applied in previous sections, that were included in dynamic simulation models.

- Maximum fault throws of 30 meters should be considered for the sub-seismic faults. Throws lower 30 meters can't be identified due to 2D/3D average vertical resolution.
- Average fault length was determined using throw vs. length correlations. As a result, lengths are estimated to be in the orders of 1:10 to 1:100, meaning that, sub-seismic faults with a throw of 30 meters, could have a length that ranges between 300-3,000 meters.
- Sub-seismic fault frequency is very low. According to the correlations, frequency of this kind of faults could be 1 fault per every 10 km.
- Shale gauge ratio (SGR) values between 2-45 were obtained for fault throws less than 30 meters for the injection zone. SGR values above 20-25 are considered good seals, so in this case for sands with low throw it would be possible not to have complete fault seal.
- Using calculated SGR values, transmissibility values between 0.15 and 0.7 were calculated for sands with low throw, with an average transmissibility value of 0.2 were obtained for these kinds of faults.

Previous estimated parameters for sub-seismic faults were included in the geological models but these parameters were no always limited to these values. Fault dimension were pushed above the high ranges with the purpose of driving the models to failure.

3.1.1.4 Saturation functions

When no real data is available through lab tests, neither analog data is obtained, well-known correlations can be used to obtain saturation curves for each of the interpreted facies of the static model. Several authors (Brooks & Corey, n.d.; El Sharawy & Gaafar, 2019; Ghomian et al., 2008; Holtz, n.d.; Kozak et al., 2005; Van Genuchten, 1980) have developed correlations based on experimental data to obtain kr and Pc curves using petrophysical calculated values such as porosity, permeability, grain size distribution, among others. After an extensive literature review, several correlations that can be used in CCS projects were obtained and applied in this study.

Using all the information obtained from literature, the following workflow was developed to generate kr and Pc curves for dynamic simulation purposes when no real data or analog data is available.

Capillary curves calculation:

To calculate the capillary curves for each facies, Brook's and Corey (Brooks, 1965) or Van Genuchten (Van Genuchten, 1980) models can be used. For this study, Brook's and Corey model was used for Pc calculation. The capillary pressure is given by the following equation:

$$P_c = P_d \times S_w^{*\,-1/\lambda}$$

Where:

$P_d = Threshold\ Pressure\ (psi)$

$S_w^* = \frac{S_w - S_{wir}}{1 - S_{wir}}$

$\lambda = Pore\ size\ distribution\ index$

Calculation of the threshold pressure P_d , irreducible water saturation S_{wir} and pore size distribution index are required to calculate the capillary pressure curve.

Value of threshold pressure can be calculated using the Berg equation (Berg, 1975) modified for the CO_2-H2O system:

$$P_d = 16.3 \times \frac{IFT}{D\_mm}$$

Where the IFT is the interfacial tension in N/m; According to (Meckel, T.A., 2010), this value for a CO_2-H20 system can be assumed as 30 mN/m. D_mm is the grain diameter given in mm, values for grain diameter for different facies can be obtained from Figure 14 elaborated by (Meckel, 2015). The figure presents values of median gain diameter for different sands of 54 geologic sandstones facies used in flow simulation.

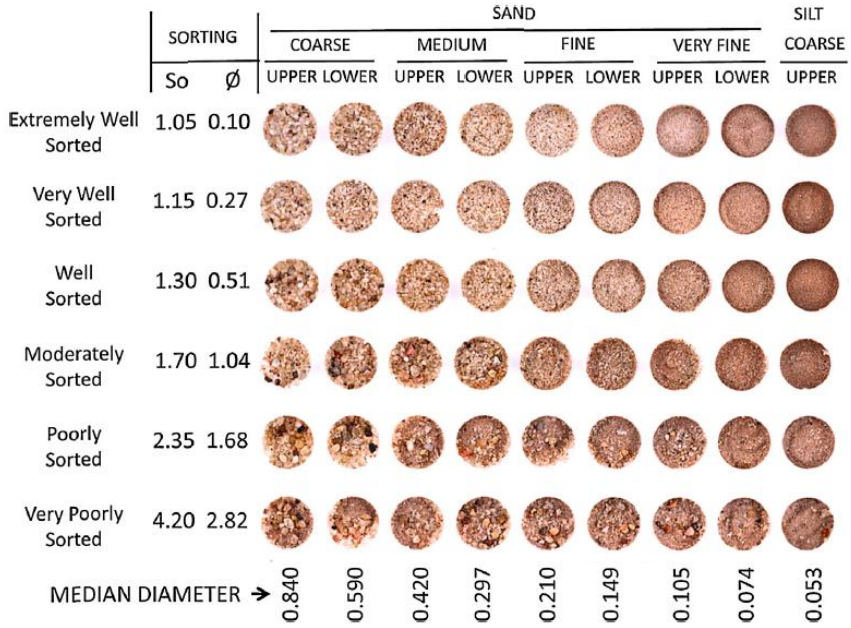

Figure 14. Grain diameter for 54 geologic samples (Meckel, 2015)

For this study values for medium sand, fine sand and silt were used to calculate the threshold pressure of the facies used in the dynamic model.

To calculate S_w^*, the irreducible water saturation needs to be obtained. Several authors have developed correlations to calculate the S_w^* using porosity and permeability values using experimental data from around the world. Is important to mention that most of these studies were developed using sandstone samples and the correlations work fine in those facies, meanwhile, some of them can't be used in shale facies. For this study (Timur, 1968) correlation was used due to the applicability in sandstones and shale facies. The irreducible water saturation S_{wir} for each facies is calculated using the following equation:

$$S_{wirr} = 3.5 \times \frac{\emptyset^{1.26}}{k^{0.35}} - 1$$

Average values of porosity and permeability for each facies should be provided during the static modeling stage. For this study, three (3) faces were assumed to include in the static model. Table 2 contains the values used in the S_{wir} calculations:

Facies	Porosity (Fraction)	Permeability (mD)
Medium Sand	0.30	3,152.5
Fine Sand	0.14	24.0
Shale	0.07	0.3

Table 2. Porosity and Permeability values for each facies in the simulation model

The last parameter that needs to be addressed before the P_c calculation can be done, is the pore size distribution index (λ). This is a value that can be experimentally obtained if real data is available, meanwhile, if no data is offered, according to (Baker, 2015) and (Kozak et al., 2005), values between 0.1 and 0.5 can be used for different facies, values close to 0.5 for medium sandstones and values close to 0.1 for shale facies.

Using all the previous information, P_c curve for each facies can be calculated. For this study, three (3) different capillary pressure curves were generated and are presented in Figure 15:

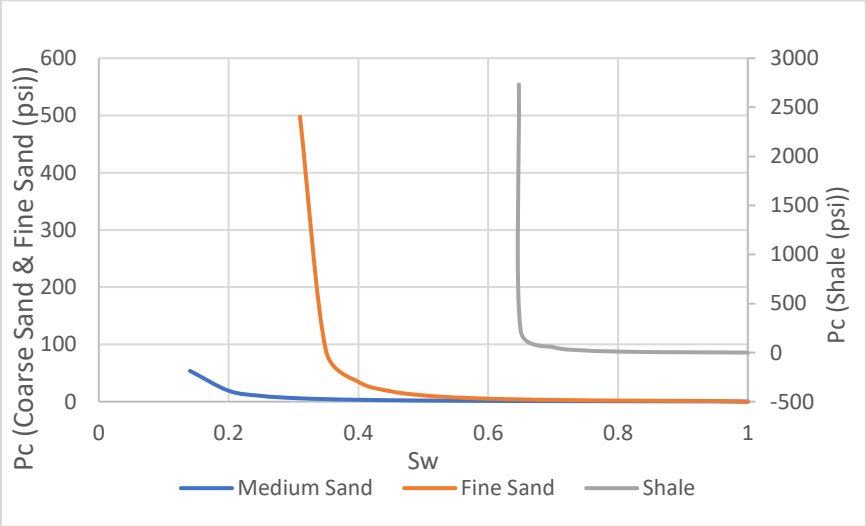

Figure 15. Capillary Pressure curves for each facies used in the simulation models

Relative Permeability curves calculation:

For this study, the following Corey's model equations was used to determine the relative permeability curves:

$$k_{rg,dr} = k_{rg,max} \times \left(\frac{S_g - S_{gc}}{1 - S_{gc} - S_{wir}} \right)^{n_g}$$

$$k_{rw,dr} = k_{rw,max} \times \left(\frac{S_w - S_{wir}}{1 - S_{wirr}}\right)^{n_w}$$

Where:

$k_{rg,dr}$: Gas relative permeability during drainage process

$k_{rw,dr}$: Water relative permeability during drainage process

$k_{rg,max}$: Maximum gas relative permeability @ S_{wir}

$k_{rw,max}$: Maximum water relative permeability @ S_{gc}

S_{gc}: Connate gas saturation

S_{wir}: Irreducible water saturation

n_g and n_w: Corey's exponents

There are different methods to determine the main parameters required for relative permeability curves' calculations. Most of those methods are based on experimental data and core lab experiments. For this study, Table 3, taken from literature (Hosseini et al., 2024), was used as a guidance for CO_2-brine relative permeability calculations.

Drainage	n_w	3.5 – 7
	n_g	1.5 – 3
	$k_{rg,max}@S_{wir}$	0.8 – 1
	$k_{rw,max}@S_w = 1$	1
	S_{gc}	< 0.05
Imbibition	k_{rw}	Follow DRN, no hysteresis
	n_g	1.5 – 3
	Land C for S_{gt}	1.1 – 3.3
Reference permeability	k_{ref}	$k_w@S_w = 1$

Table 3. Corey's parameters for relative permeability calculations (Hosseini et al., 2024)

For this study, the S_{wir} for each facies was calculated using the (Timur, 1968) method that was also implemented for P_c calculations. The rest of parameters were obtained from the previous table. Using all the information available and Corey's equations, different permeability curves were generated for each of the facies used in the model. As a reference, Figure 16 presents one of the sets of relative permeability used in this study.

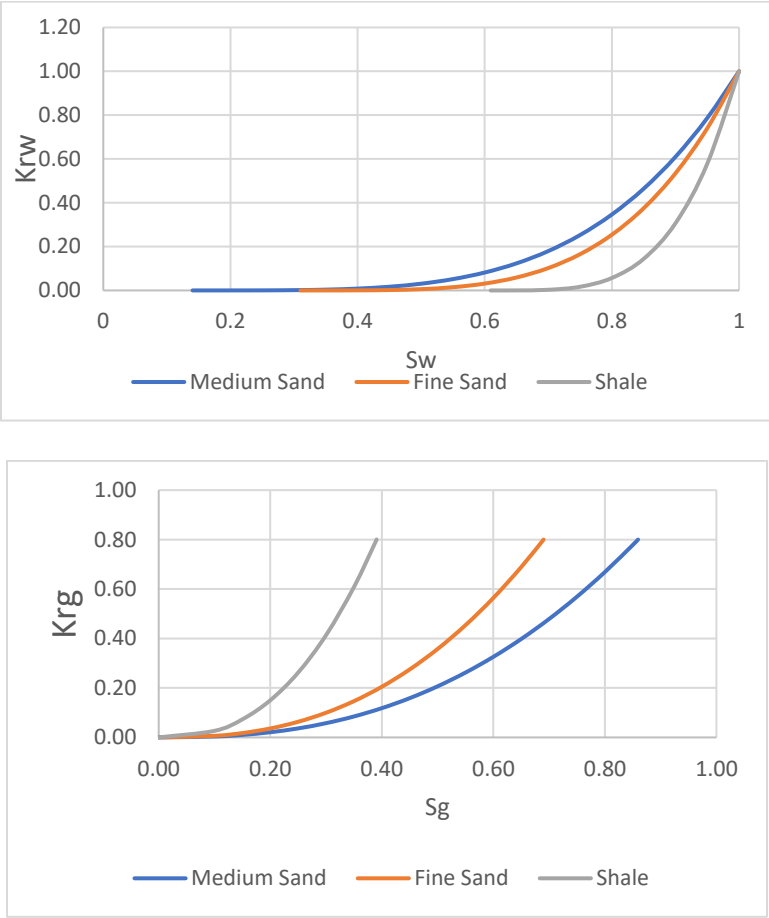

Figure 16. Example of Relative Permeability curves used in the simulation models

3.1.1.5 Critical pressure calculation

To define pressure front, critical pressure (or threshold pressure according to EPA guidelines) has to be calculated. According to Nicot et al. (2009), critical pressure is defined as the minimum value of pressure increase sufficient to lift denser brine up an open wellbore to the

base of the USDW aquifer. The following equation will allow to calculate the critical pressure in a reservoir:

$$\Delta P = g \times \frac{\varepsilon}{2} \times (Z_u - Z_i)^2$$

Where:

ΔP= Critical pressure

g= gravity

ε= density gradient, a linear coefficient depending on the salinity increase with depth, and also geothermal gradient.

$\varepsilon = \frac{\rho_u - \rho_i}{Z_u - Z_i}$

ρ_u= Fluid density at USDW

ρ_i= Fluid density at the injection zone

Z_u= Depth of the top of the injection formation

Z_i= Depth of the base of the USDWs.

With this equation, a critical pressure of 150 psi was calculated. This value will delimitate the pressure front that will be presented in these results. If the pressure is equal to or higher than 150 psi compared to the original reservoir pressure, water could flow from the injection zone to the USDWs.

Additionally, EPA guidelines define AoR by the union of the pressure front (defined by the critical pressure as previously mentioned) and the CO_2 saturation plume. The union of these two areas will give the total AoR to be presented through this study. Figure 17 presents an example of CO_2 plume, pressure front and total AoR for clarification:

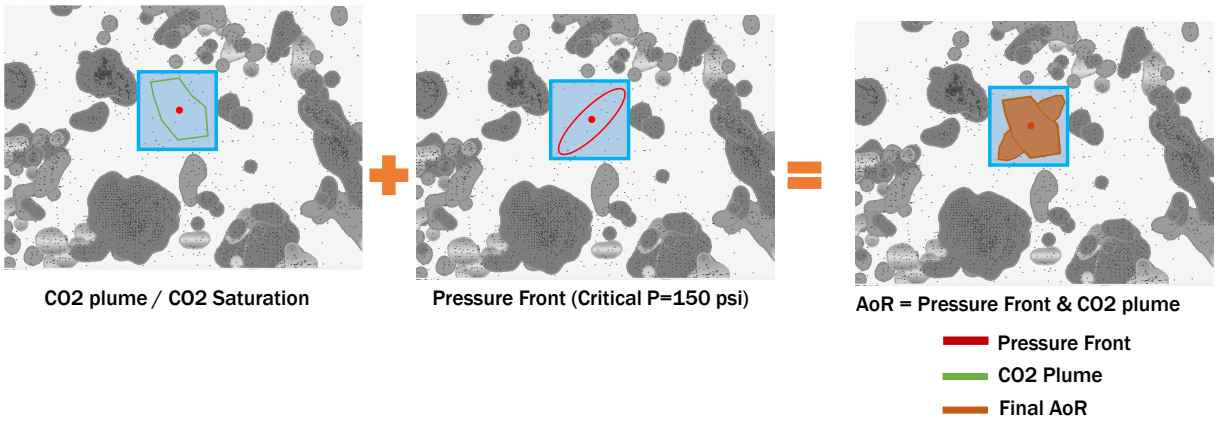

Figure 17. Area of Review (AoR) definition

3.1.2. Box model definition

For a first-pass exploration of parameters and sensitivities, a simple box model with one channel and one fault was built (Figure 18).

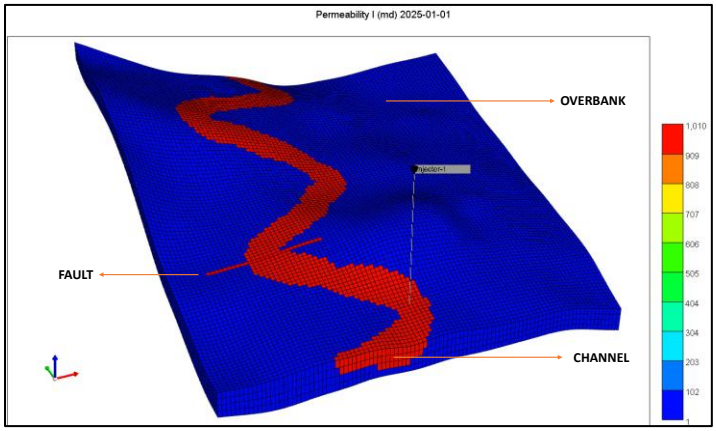

Figure 18. Box Model – Permeability map

Structural maps obtained from a project were taken to build the model, and a small portion of the area of interest was modeled. This is a 10x10 km model with 100 grid cells in the x and y direction (100 ft for DX and DY), 120 ft thick with four layers in the z-direction (30 ft for DZ). A permeability value of 1,000 mD was assigned to the channel (in red in the previous figure), this value is coherent with typical permeability values obtained in previous sections for the GOM area. Length of the fault is 3,000 meters and 30 meters thick (penetrates the entire grid);

these values were selected considering the length vs. throw correlation previously presented in Figure 12 for the sub-seismic faults.

Different sensitivities were performed to understand the impact of reservoir heterogeneities in CO_2 fluid flow behavior using this simple configuration. Sensitivity cases were run varying fault transmissibility values using the following values (0.001, 0.01, 0.1, and 1). Overbank permeability (in blue in the previous figure) was also varied in orders of magnitude from 0.1 to 100 mD.

Two facies were used in this model, medium sand (for the channel) and for the overbank facies, depending on the permeability assumed for those facies, different relative permeability and capillary curves were used. For overbank permeabilities of 0.1 and 1 mD, a shale facies was assumed; for permeability of 10 mD, a fine sand facies was used. For overbank permeability of 100 mD a medium sand facies were assumed.

3.1.3. Realistic single flow-unit model definition

To experiment with more realistic geology without incurring the computational expense of a full-scale 3D mode, a new generation of single flow-unit models were built by Dr. David Hoffman, an experienced geomodeler working at the Bureau of Economics Geology (BEG) and actively involved in this project. Real data related to structural maps, wellbore data, core data, and regional information from the unnamed project (unnamed due to confidentiality), as well, as the information obtained in previous sections were used to generate these models. The section below describes how Dr. Hoffman built the model.

Generated models should be able to identify the primary behavior of the CO_2 plume for one flow unit in the presence of a channelized reservoir and sub-seismic faults networks at different length directions. A stochastic approach was used to generate several geological models to include uncertainties related to channel size and connectivity

To build the models, information on 153 wells was included. Petrophysical data in the form of curves designated as the final and most reliable petrophysical interpretations for a given well were used. Curves of effective porosity, total porosity, permeability, and Vshale were available for this study.

Lithofacies data from well logs were not available at the time of construction of these models, so a synthetic facies property log was built from the sand volume. Vsand was obtained from Vshale by inverting the Vsh curve (considering carbonate to be negligible due to the geological environment in the area of interest).

Realistic single flow-unit model - Structural Framework and Grid model

Original structural framework for the project was provided by the operator. This framework included seismic faults as well as various horizons and wells within the area of interest. The original grid dimension was 143 x 189 x 231 cells (6,243,237 cells in total), with a cell dimension of 500 ft in the *x* and *y* direction and 19 ft in the *z*-direction.

To build a realistic but flexible model, one single flow unit of the structural framework was considered. This flow unit has a 200 ft thickness and 10 layers. This unit has been considered by the operator as one of the injection zones during the CCS project due to its petrophysical characteristics. The used models have 143 x 189 x 10 cells (270,270 cells in total).

To create a simple model to mimic the possible ranges of channel belts, available published information was used to develop four end-member cases for simulation purposes.

Each of these cases utilizes data ranges for channel geometry obtained from amplitude extractions coming from 3D seismic and literature, as it was explained in previous sections. This information was used to incorporate hypothetical meandering fluvial trends in the models.

Each of the models was constructed using a spherical variogram with hypothetical major-minor axis parameters that were based on the published data. A NW-SE regional depositional axis was considered, so a variogram azimuth of 315 was implemented in all cases. Sinuous polylines

were digitized through the area using the general amplitude and wavelength parameters obtained. These polylines were then used to create a probability map that could be used to condition property distribution as is shown in Figure 19.

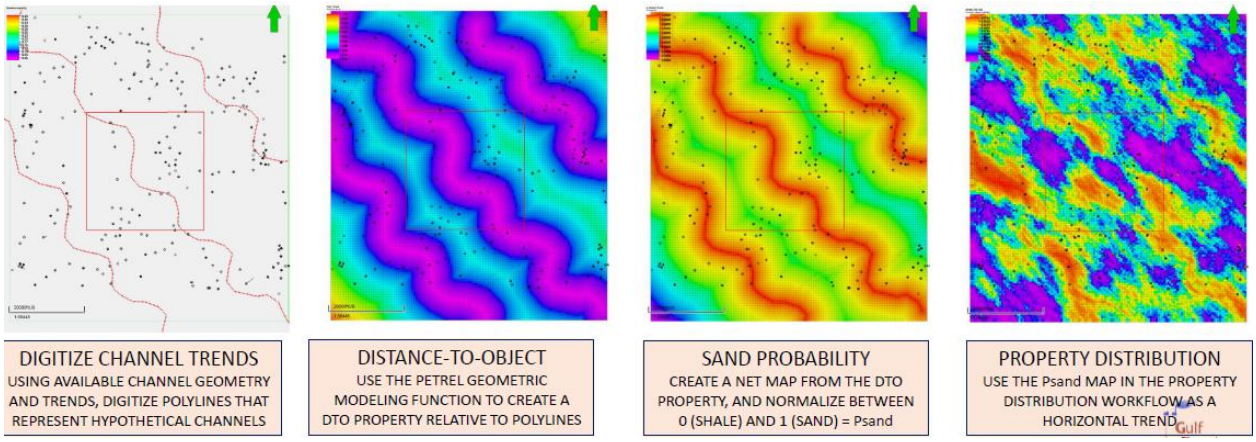

Figure 19. Workflow of including channel trends in the geological models used in this study

As shown in the 2D view of sand percentage (far right map), the revised property distribution using the channel probability to "steer" well data in the 3D distribution appears geologically realistic.

The following four geological cases were generated (Figure 20):

CN-2 – Continuous, narrow channel systems
CW-2 – Continuous, wide channel systems
DN-2 – Discontinuous, narrow channel systems
DW-2 – Discontinuous, wide channel systems

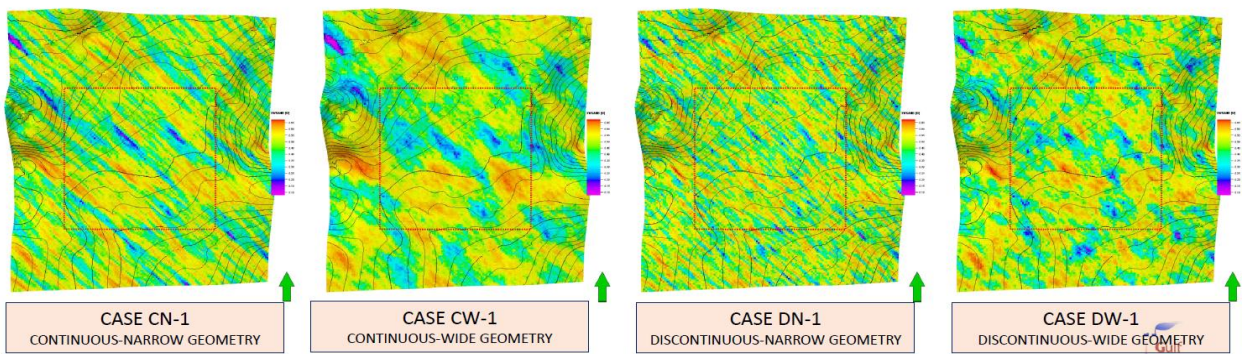

Figure 20. Sand volume of the four geological models constructed for this study

Realistic single flow-unit model - Property Modeling

Basic geometric properties (Layers, Zones, and Regions) were created without adjustment to the vertical layering provided by the operator. Continuous petrophysical properties from the operatory-provided curve logs were upscaled into the 500' 3D grid model using a mid-point pick methodology. As previously discussed, a sand volume log was not available for a statistically significant number of wells, so a derived sand percentage log was created from the Vsh log since the data indicates that carbonate components are an extremely minor fraction of the total lithology in most wells.

For the sand percentage property, because the property distributions and synthetic facies distributions use the sand volume property to condition the 3D property, it needed to be done first. The Vsand property was created by upscaling the Vsand from Vshale log into the 3D grid in the injection zone and then distributed using a sequential Gaussian simulation (SGS) algorithm. The input data distribution was distributed in the data analysis module using the input well-log data as the basis for the distribution. In the petrophysics property module, the input variograms derived for each case were used with the data distribution from data analysis, and the property was collocated co-kriged with the horizontal probability trend derived from sand volume.

Lithofacies logs were not available at the time these models were created, but to provide the flexibility to test the effects of rock-type specific properties, a pseudo-facies property was created. Assuming that the Vsand log derived from Vshale could be used as a proxy for rock type, the Vsand distribution was used to create four rock types based on Vsand range:

- Shale – 0.0 < Vsand < 0.35
- Silty Sand – 0.35 <= Vsand < 0.50
- Fine Sand – 0.50 <= Vsand < 0.57
- Coarse Sand – Vsand => 0.57

These Vsand percentage ranges were derived empirically from the distribution histogram (see Figure 21).

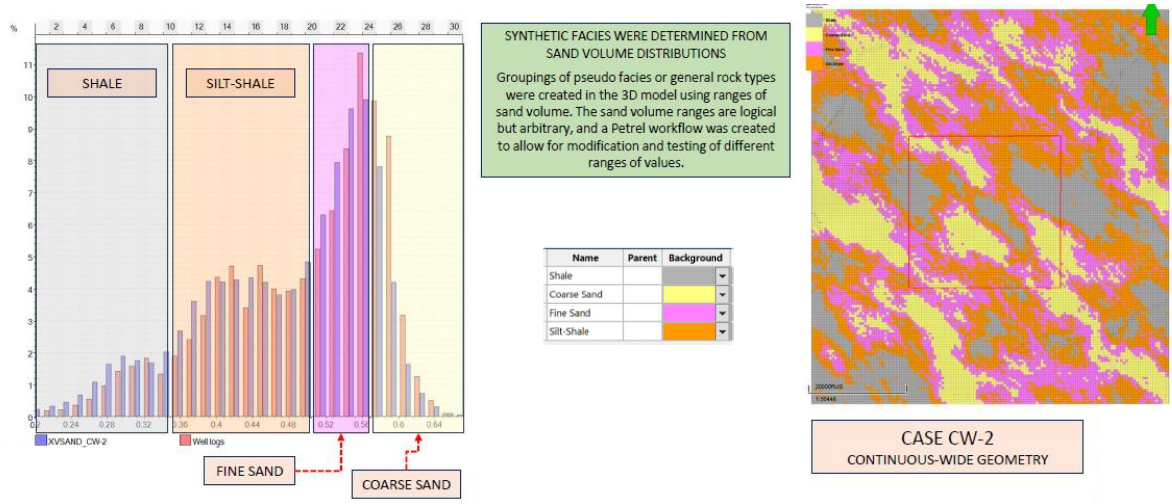

Figure 21. Lithofacies modeling – Continuous Wide geometry model

For the porosity modeling, The PORE (effective porosity) curve available was upscaled into the 3D grid in the injection zone and then distributed using a sequential Gaussian simulation (SGS) algorithm. The data distribution was done in the data analysis module using the input well-log data as the basis for the distribution. In the petrophysical modeling process of Petrel Software, the input variograms derived for each case were used directly, the distribution from data analysis, and the property used the horizontal probability trend derived from sand volume as a secondary variable. Collocated co-kriging used the net sand map from the VSAND property as a surface coefficient. There did not appear to be significant differences between the PORE (effective porosity) and PORT (total porosity), so the total porosity property was not modeled in this case.

For the permeability modeling, The K curve available was upscaled into the 3D grid in the flow unit zone and then distributed using a sequential Gaussian simulation (SGS) algorithm. The data distribution was done in the data analysis module of Petrel, using the input well-log data as the basis for the distribution. In the petrophysical modeling process of Petrel, the input variograms derived for each case were used directly, the distribution from data analysis, and

the property used the Vsand property volume as a secondary variable. Collocated co-kriging used the net sand map from the Vsand property as a surface coefficient.

Resulting models with lithofacies, porosity, and permeability maps were used as main input parameters for each of the four models. Four geological models were generated in this stage to include geology uncertainty in the study and try to determine the possible outcomes during CO_2 injection projects.

Additionally, "model faults" were generated with the aim to be included in the simulation models. Four sets of experimental faults were generated based on the fault characterization work. To investigate the end-member of maximum impact, fault dimensions (length, throw, etc.) were pushed to the upper realistic limits of sub-seismic faults. These faults were generated with the aim to evaluate the worst-case scenarios. Faults with 0, 45, 90, and 135° directions were constructed. This helped to include sub-seismic uncertainties in the generated models (Figure 22).

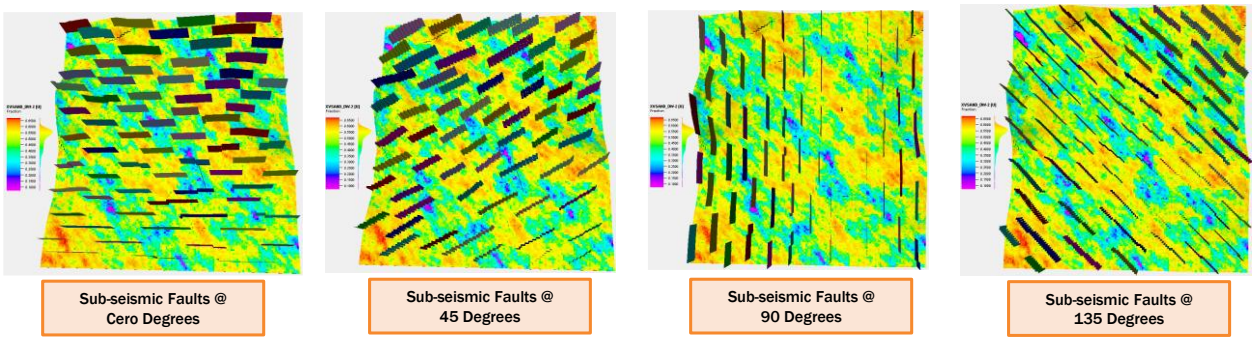

Figure 22. Sub-seismic Fault networks used for each of the geological models

Lastly, transmissibility values from zero (0) to 1 were assigned to those sub-seismic faults to investigate the full range of possible impacts (not all of which are realistic for sub-seismic faults). With these parameters, a total of 64 models were generated for dynamic simulation purposes. Four geological models with four sub-seismic fault distribution/direction and four different transmissibility values were assumed for those cases (Figure 23).

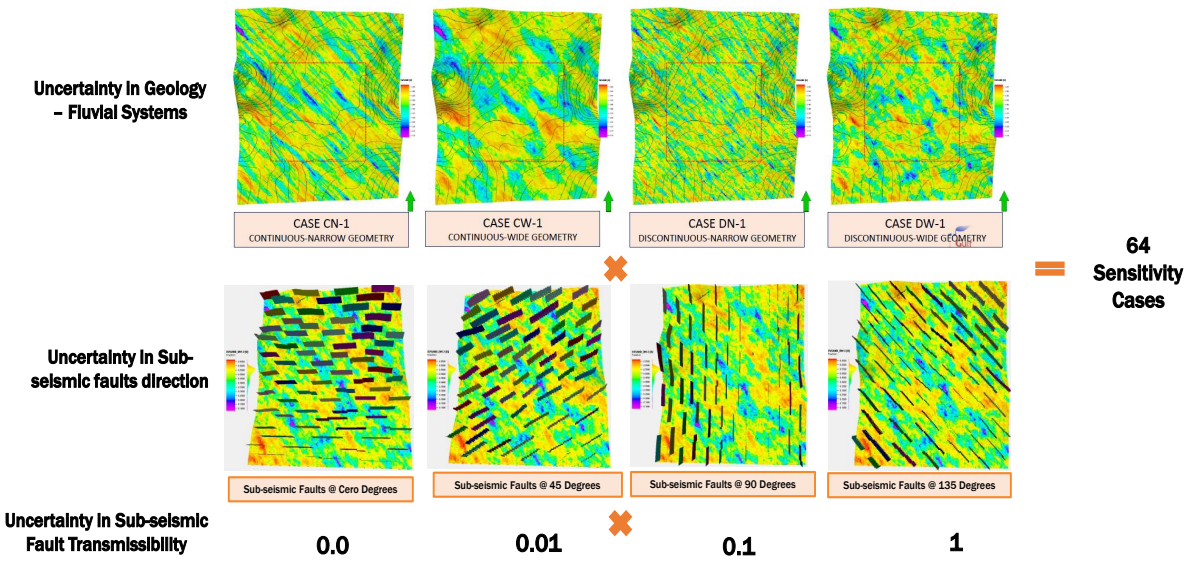

Figure 23. Realistic but flexible models' experiments setup

3.1.4 Full-field model definition

Finally, we used a full-scale 3D reservoir model to test our preliminary conclusions. This model was built including all the flow units of the Miocene injection zones, as well as the sealing unit on the top of the Miocene formation. Real data related to structural maps, wellbore data, core data, regional information analysis, amplitude extractions, lithofacies analysis, among other information was included in the model generation.

To build the model, information on 153 wells was also included. Petrophysical data in the form of log curves designated as the final and most reliable petrophysical interpretations for a given well were used. Curves of effective porosity, total porosity, permeability, and Vshale were available for this study.

Lithofacies data was derived from SP curves. This work was done by Dr. David Carr and Dr. Carlos Uroza, experienced BEG researchers working on this project. Facies definitions were adjusted using real core data for calibration. In addition to the core calibration, refinement of the facies categories was performed to include the following log-based lithotypes: Red Shale, Mudstone, Siltsone, Sandstone, and Limestone.

Data generated includes discrete lithology logs based on the SP and GR curves. The GR-derived lithofacies were used in the 3D grid due to the reliability of the GR data.

Full-field model - Structural Framework and Static Grid model

Original structural framework for the unnamed project was provided by the operator. This framework is the same used for the previous models and includes seismic faults, as well as, various horizons and wells within the area of interest. The original grid dimension was 286 x 318 x 200 cells (18'189.600 cells in total) with a cell dimension of 250 ft in the *x* and *y* direction and 14 ft in the *z*-direction. Injection zones were refined in the z direction to have better detail during the dynamic simulation stage.

During the first approaches to create a static model, some property anomalies were discovered when the static model was exported from Petrel and then imported into the CMG Software. These anomalies were related to the faults in the structural framework. To eliminate the gridding and property distribution artifacts in the vicinity of framework faults, a static model without the framework faults was created from the original grid.

In order to include the faults, simulation faults were used. These faults closely approximated the original framework faults while not creating the 3D grid distortion observed before. To generate the simulation faults, the original framework faults were converted to surfaces and then intersected with one of the injection horizons, thus creating a polyline at the intersection. Once the fault polylines were generated, a set of simulation faults was created.

Full-field model - Property Modeling

Continuous petrophysical properties from petrophysical log data provided by the operator were upscaled into the 250 feet grid cell using a mid-point pick methodology. Discrete property data (i.e., lithofacies) were upscaled into the model using a standard "most of" upscaling.

All continuous petrophysical properties were evaluated using Petrel Data Analysis tools. A vertical proportion curve and probability curve were created for facies by zone. For continuous properties, data transform distributions were created by facies in each zone. Detailed

variograms were not constructed, but a general N-S variogram with a 2:1 major-to-minor axis ratio was used as a preliminary estimate, and then refined with the depositional trend lines obtained from amplitude extractions.

Upscaled lithofacies logs provided were distributed into the 3D grid using a Sequential Indicator Simulation (SIS) algorithm, with the distribution conditioned with a probability trend map generated from depositional trend lines interpreted by Dr. Carlos Uroza. The trend line polygons and derived probability maps used as horizontal trend surfaces were generated for each zone in the Lower Miocene section as geometric distance-to-object properties.

The facies distributions derived using this methodology were then used to condition and distribute the petrophysical properties. Lithofacies were distributed in the geomodel using a basic workflow, that incorporates a combination of interpreted environments of deposition from well log cross-sections, amplitude extractions from 3D seismic, and interpretations of sand distribution and geometries provided. The general workflow used during the model generation is described in Figure 24:

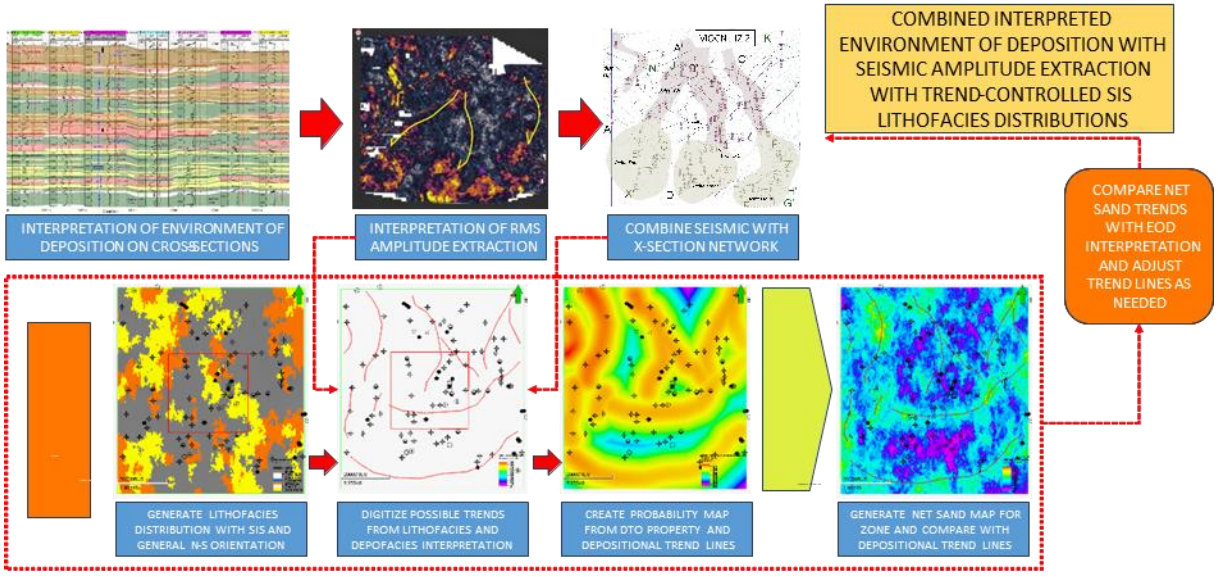

Figure 24. Workflow for Static Modeling – Full-field model (Provided by Dr. David Hoffman, BEG, 2024)

Continuous petrophysical properties in the fine grid (250’ x 250’) were modeled using the lithofacies property distributions to condition property distribution. Total and effective porosities (PORE and PORT) were upscaled and distributed using Sequential Gaussian

Simulation (SGS) algorithm, with the property conditioned by lithofacies. Permeability was generated following the same procedure used for the porosity with the property also conditions by lithofacies and collocated co-kriging to PORE as a secondary variable.

As a result of this workflow, a static model with effective porosity, total porosity, permeability in the x direction, and facies properties was generated (Figure 25).

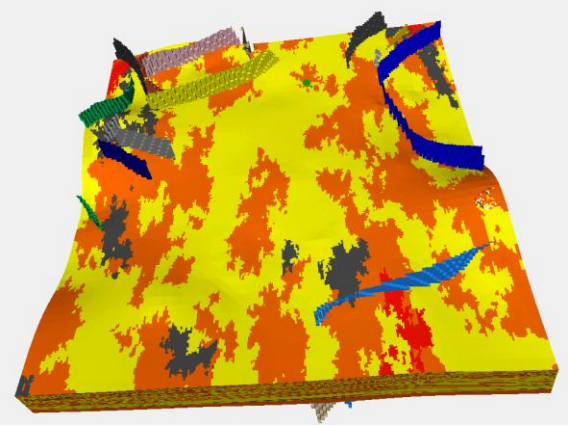

Figure 25. Static Modeling – Full-field model (Provided by Dr. David Hoffman, BEG, 2024)

Full-field model - Model calibration with well test data

As a part of the static model calibration, step rate test (SRT) data obtained from the operator in one of their stratigraphic wells (Figure 26) was used to calibrate the reservoir permeability of the model.

Bottom hole pressure, as well as, injection rates from the SRT test were included in the model. History match of that data was performed modifying the permeability values of the original model.

As a result of this procedure, a permeability multiplier was applied to the entire model in order to calibrate the observed bottom hole pressure to the one obtained in the dynamic model (red dotted lines in Figure 26). At the same time, permeability values calculated during pressure build-up interpretation were compared with the ones obtained after the model calibration to make sure similar values were being used.

After this final calibration was performed, the static model was exported to CMG Software to proceed with the dynamic simulation.

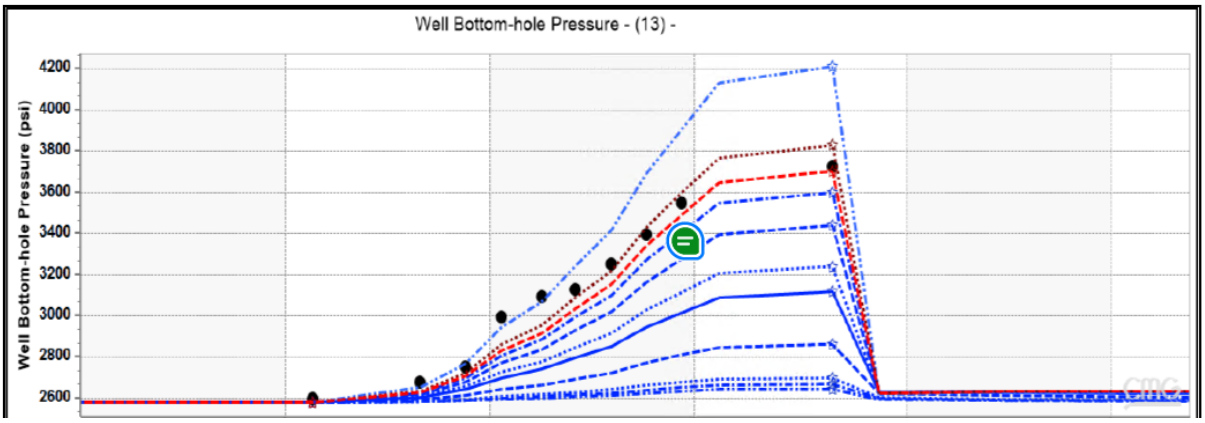

Figure 26. Step Rate Test – History Match, Static Model (Real data in black dots, simulated data in blue and red lines)

Dynamic Simulation Model Setup

The static model was exported as a rescue file from Petrel and then imported into the Computer Modeling Group (CMG) Software for dynamic simulation.

In order to set up the simulation model, the cell's dimensions were kept with the same dimension as the static model. Three facies with their corresponding relative permeability curves and capillary pressures were generated.

The operator of the project provided a set of relative permeability curves for one of the facies, so the correlations generated using the workflow mentioned in section 5.1.1.3 were calibrated with this data. Values of the constants used in (Timur, 1968) for irreducible water saturation were slightly modified to obtain a value similar to the one provided by the operator (value of the k exponent changed from 0.35 to 0.25). Additionally, values of Nw and Ng recommended by (Hosseini et al., 2024) used for relative permeability curves calculations in Corey´s equation were also calibrated with the real data (Nw=3.3 and Ng=2.5 used). It is important to mention that relative permeability values obtained before the calibration were similar to the ones

obtained in the lab, so if no information is available, the workflow provided in section 5.1.1.3 can be used for relative permeability and capillary pressure curves generation (Figure 27).

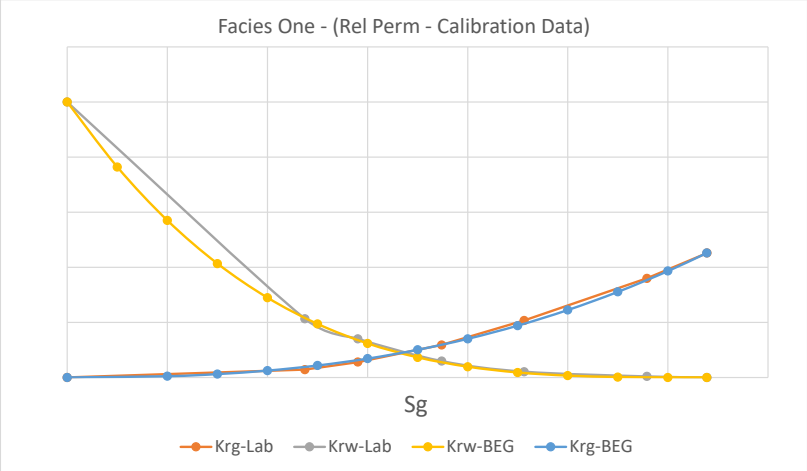

Figure 27. Relative Permeability Curve – Facies One

For the simulation model, closed boundary conditions were used, where boundaries were extended out using volume modifiers. Volume and transmissibility modifiers were applied in the outermost cells in the grid following the recommendations provided by (Hosseini et al., 2024). The code used to include the extended closed boundary conditions in the model is described in the Appendix II.

For the full-field model, three (3) injection wells were created. Injection rates varied for each well and a period of 15 years of injection was simulated, as well as, 50 years post-injection period was included.

CO_2 injection was achieved through the perforation of different intervals within the Miocene injection formation, limiting the injection by the maximum allowable pressure (90% of the fracture pressure of the injection formation).

Finally, sub-seismic faults with a zero-degree angle were included in the full-field model to evaluate the impact of these faults in the AoR, CO_2 plume, and pressure front. Sensitivity in the fault transmissibility was included for these models.

4. CHAPTER IV

In this chapter, results obtained in the dynamic simulations will be presented and analyzed and consequences of unintended CO_2 migration due to sub-seismic faults will be quantified. Avoiding unintended migration in complex environments will require additional investment strategies. Operators are concerned about the additional cost associated with low injection capacity, high injection pressure, migration out of the current lease, and additional monitoring costs. These results will give some insights related to the main parameters that could cause an unintended lateral migration CO_2 during CCS projects and will help operators minimize those risks through a better reservoir characterization strategy.

4.1. RESULTS AND ANALYSIS

4.1.1. Box Model - Results

Results of the sensitivity analysis are shown in the map view in Figure 28, with increasing fault transmissibility from left to right and increasing overbank permeability from top to bottom. Channel is located in the north-south direction in the middle of the model and fault is presented as a dotted red line in the west-east direction. Variations of sub-seismic fault transmissibility and overbank permeability are the main variables. Figures of AoR, (union of CO_2 saturation plume and pressure front) are the outputs presented for each case in Figure 28:

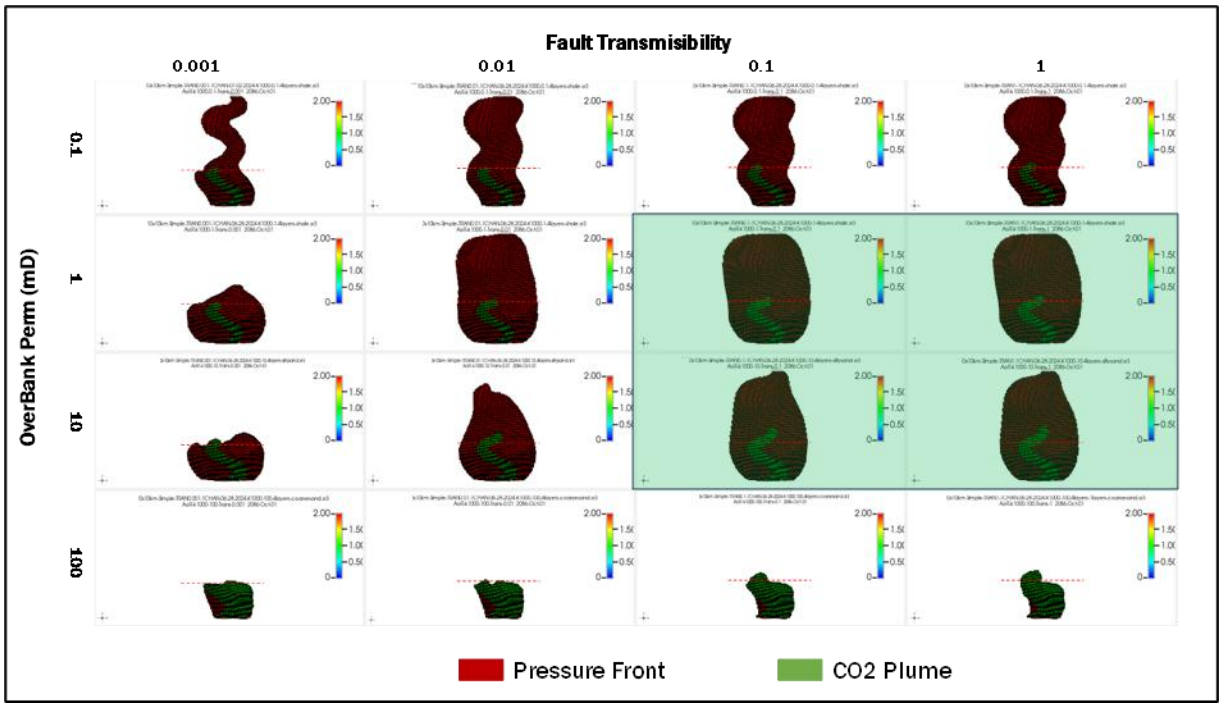

Figure 28. AoR – Box model – (CO_2 Saturation in green – Pressure front in red – Green rectangle shows realistic values of overbank permeability & Fault transmissibility)

As shown in Figure 28, AoR is most sensitive to variations in overbank permeability. The higher the overbank permeability, the smaller the AoR due to pressure dissipation in the overbank formation. Meanwhile, pressure is dissipated in the overbank formation even when the overbank permeability is very low. The size of the AoR is impacted mostly by the pressure front when low values of overbank permeability are used, on the other hand, AoR is impacted mostly by CO_2 plume when overbank permeability is high.

Fault transmissibility play a role in CO_2 migration keeping most of the CO_2 in the south part of the model. No big effect on the AoR is observed when values of transmissibility higher than 0.1 are used. Box model results show that fault transmissibility only plays a role when very low values of transmissibility are used (0.001). Figure 28 also shows that fault is more important when high values of overbank permeability are used. The CO_2 saturation shape (in green in the previous figure) doesn't follow the channel because once it reaches the fault it starts to migrate to the overbank formation. If the overbank permeability is small, the CO_2 stays in the channel and whenever finds the fault, it pressurizes until can pass through the fault due to capillary pressure threshold.

The green rectangle observed in Figure 28 represents the realistic values of overbank permeability and fault transmissibility, and shows that no big effect on AoR is observed when realistic values are used. Only big changes are observed for extreme case scenarios.

4.1.2. Realistic single flow-unit model - Results

In the realistic single flow-unit models, realistic values of channel geometries and petrophysical properties were used to build these models, on the other hand, hypothetical values of fault transmissibility, fault frequency and orientation were used set up the experimental models. A total of sixty-four (64) models were generated in order to evaluate uncertainty in the geology, sub-seismic fault frequency and orientation, and fault transmissibility. For each of the four geological model (four in total), different sets of sub-seismic fault orientations were used, as well, as different transmissibility values for the sub-seismic faults.

Results are also presented in matrix format, and the effect of these features (fault orientation and transmissibility) in the AoR is highlighted for easy identification purposes. In the AoR maps, the green plume is the CO_2 Saturation property with values higher than 1% and the red plume is the Pressure front (pressure change above 150 psi with respect to the original pressure).

After analyzing Figure 28, some common observations were identified:

In all cases CO_2 flow in the channel direction (SE-NW). For all the geological models, when transmissibility values of 0.1 or higher are used for the sub-seismic faults, no big effect on the AoR is observed. In those cases, the AoR is mainly driven by the CO_2 saturation and pressure does not play a big role due to the pressure dissipation in the outer boundaries of the model.

Once the fault transmissibility decreases at least two orders of magnitude or more (0.01-0.001 values), the AoR looks different. Changes in the CO_2 saturation plume shape and pressure front are observed. Faults start to play a bigger role in CO_2 migration and pressure dissipation.

Pressure seems to have the biggest effect on the AoR shape and size due to the restriction of pressure dissipation once the pressure front reaches the faults. The shape of CO_2 plume mainly follows the channel trend, but depending on the fault's orientation, pressure front will be

differently shaped following faults' orientation. The biggest AoRs are obtained whenever the cero and forty-five (0-45) degree faults are present, this is when the faults are more perpendicular to the flow direction. In none of the models, AoR reached the boundaries of the model (22 by 22 km), which implies that despite the AoR shape changes, the CO_2 and pressure don't present an extreme behavior that could impact the AoR dramatically.

Realistic values of sub-seismic fault transmissibility and orientation are highlighted in the green rectangle. In all these cases no big effect on the AoR is observed when changing the sub-seismic fault characteristics within the realistic values.

For the continuous narrow geometry geological model, Figure 29 illustrates the results obtained:

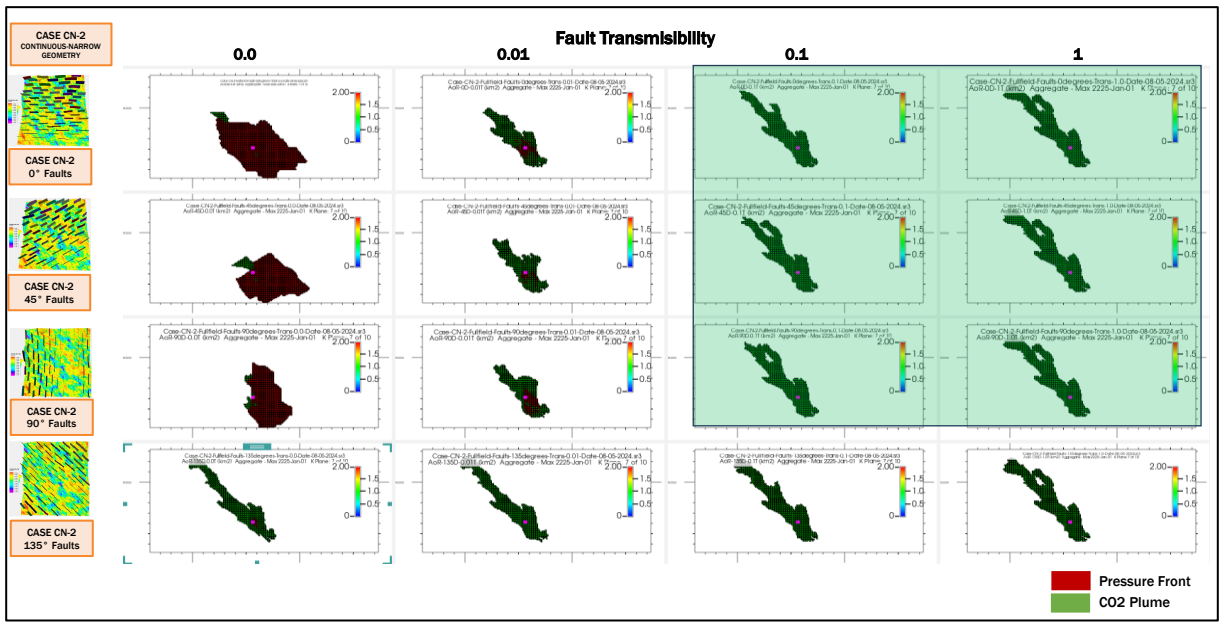

Figure 29. AoR – Realistic but flexible model – Continuous Narrow geometry geological model - (CO_2 Saturation in green – Pressure front in red - green rectangle shows realistic values of Fault transmissibility and orientation)

For the discontinuous narrow geometry geological model, Figure 30 illustrates the results obtained:

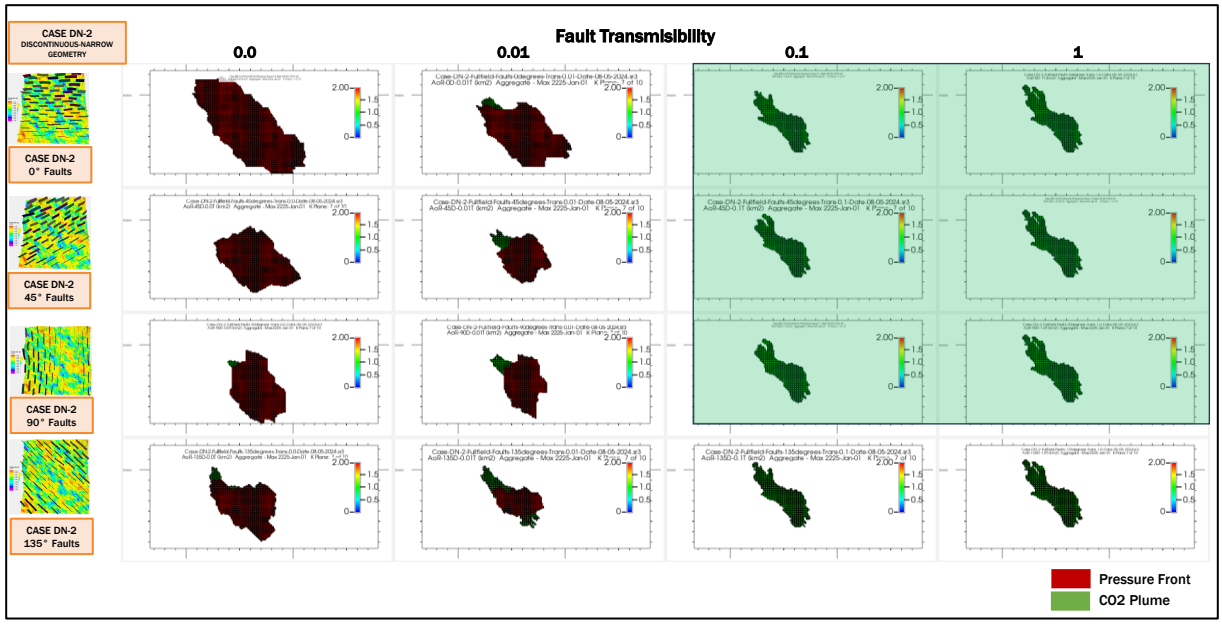

Figure 30. AoR – Realistic but flexible model – Discontinuous Narrow geometry geological model - (CO_2 Saturation in green – Pressure front in red - green rectangle shows realistic values of Fault transmissibility and orientation)

For the continuous wide geometry geological model, Figure 31 illustrates the results obtained:

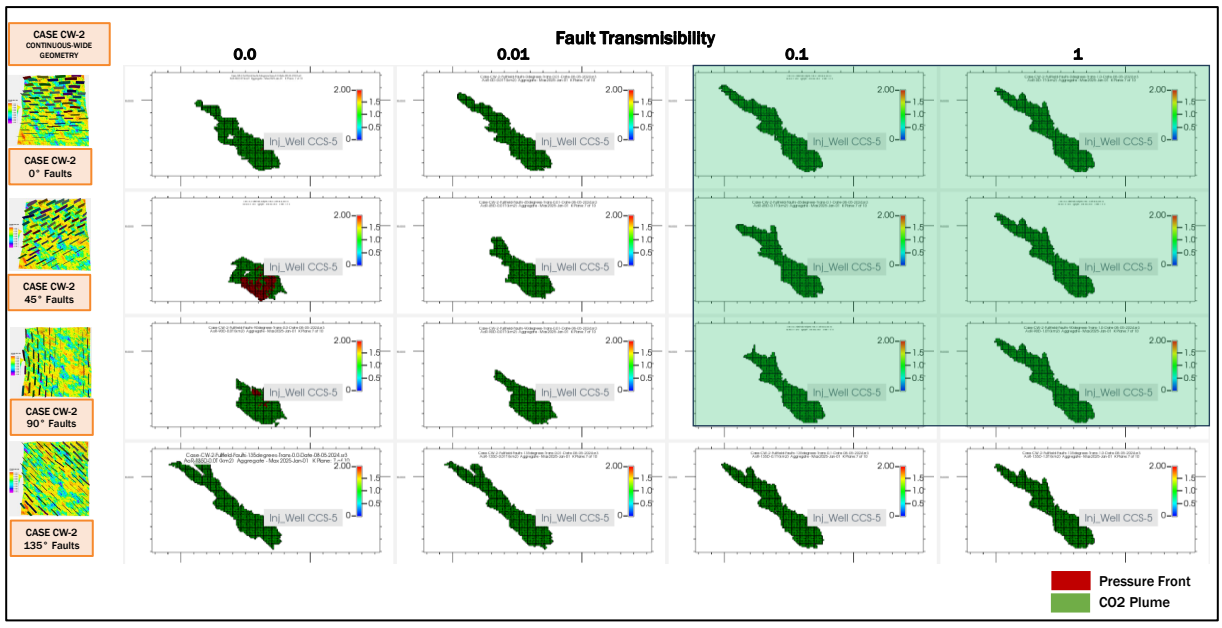

Figure 31. AoR – Realistic but flexible model – Continuous wide geometry geological model - (CO_2 Saturation in green – Pressure front in red - green rectangle shows realistic values of Fault transmissibility and orientation)

For the discontinuous wide geometry geological model, Figure 32 illustrates the results obtained:

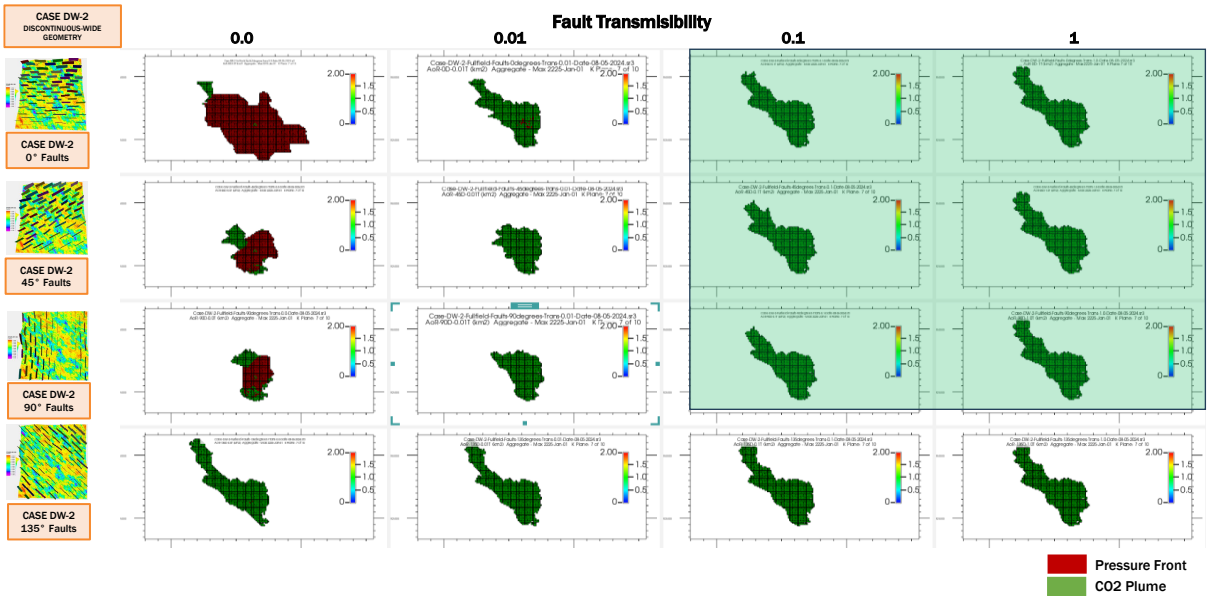

Figure 32. AoR – Realistic but flexible model – Discontinuous wide geometry geological model - (CO_2s Saturation in green – Pressure front in red - green rectangle shows realistic values of Fault transmissibility and orientation)

For reference, additional matrix figures of CO_2 saturation and pressure front for each model are included in Appendix I.

4.1.3. Full-field model - Results

Full-field model was built to evaluate the effect of the sub-seismic faults in fluid flow and CO_2 plume and pressure front in a more realistic scenario, using the static model built for this case with all the information available. Sub-seismic faults effect in horizontal and vertical CO_2 migration was evaluated.

In the base case, sub-seismic faults were not included. Several simulation cases were run to perform sensitivities. Modifications of injection rates per well, injection zones, injection times per zone, and additional perforations were considered during these simulation runs.

Figure 33 presents a map view and 3D view of the AoR obtained for the base case. For this base case, the AoR was defined by the combination of CO_2 saturations greater than 1% and pressure front with a critical pressure greater than 150 psi.

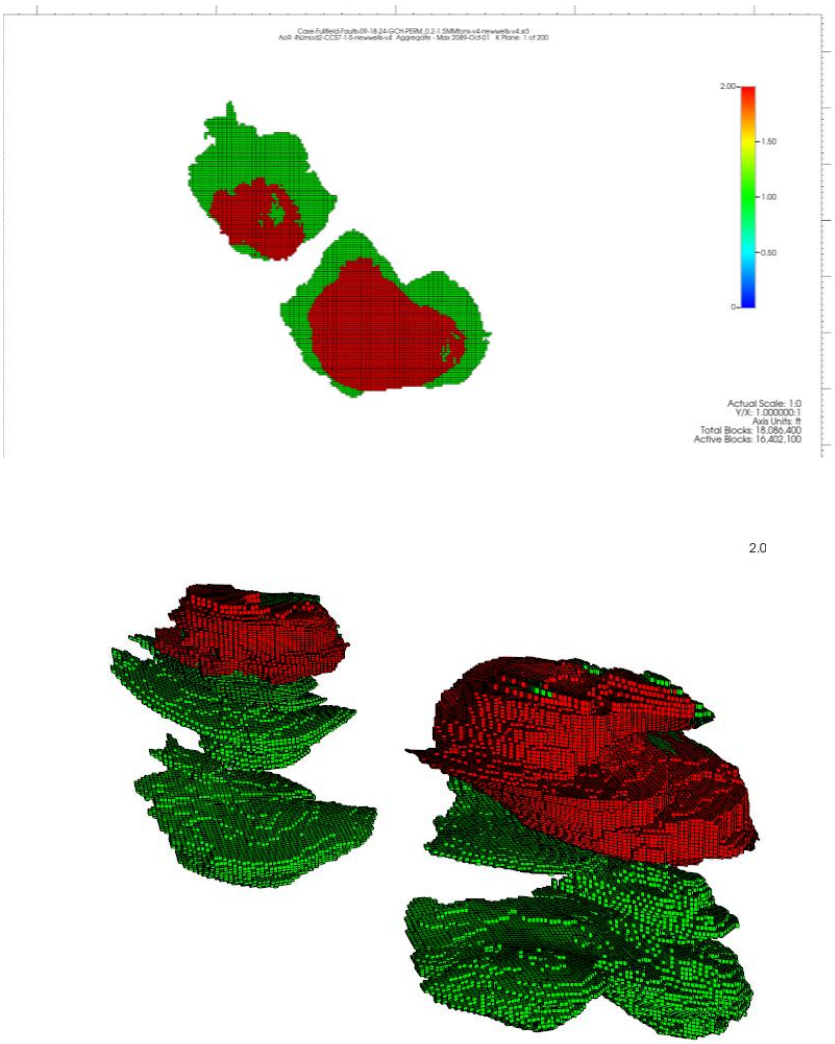

Figure 33. AoR aerial view (top) and 3D view (bottom) – Full-field model – CO_2 Saturation (in green) and pressure front (in red)- No sub-seismic faults included

In Figure 33, the AoR is mainly determined by the CO_2 saturation plume. CO_2 migrates following the dip direction of the structure (NE-SW). The pressure front seems to be inside the CO_2 plume and a rapid pressure dissipation is observed in the base case. CO_2 saturation for each injection zone seems to be mainly confined to the corresponding injection zone and no migration to the upper or lower formations was observed. CO_2 vertical migration seems to be minimal, despite the lack of regional seal between the injection zones.

The size of the AoR would fit within many of gaps between oil and gas fields on the onshore Gulf Coast area. Operators' efforts are focused to acquire a leasing area that contains the AoR, characterize possible leakage paths such as legacy wells, and define a monitoring plan inside that area, for that reason, the smallest AoR is always desired for any CCS project.

Boundary conditions are a big aspect when dynamic simulation is performed and will play a big role in the AoR size. This is why is so important for operators to identify the best boundary conditions outside the area of interest or outside the static model itself. Proper boundary conditions definition (translated in volume modifiers in the dynamic simulation) will help pressure dissipation which in fact will modify AoR size and shape. For this model in Appendix II, boundary conditions included in the CMG Software are presented. Recommended approaches of how to handle open boundaries were taken from (Hosseini et al., 2024) and included in this appendix, which could help for future studies.

After the base case was calibrated to obtain a small AoR, sensitivity analysis was performed to include horizontal "mode faults" with zero-degree orientation, 3,500 meters long, varying the fault's transmissibility from 1 down to 0.001; variations were performed in orders of magnitude. The objective of including these features is to determine how the AoR changes when "model faults" that were not initially characterized are included.

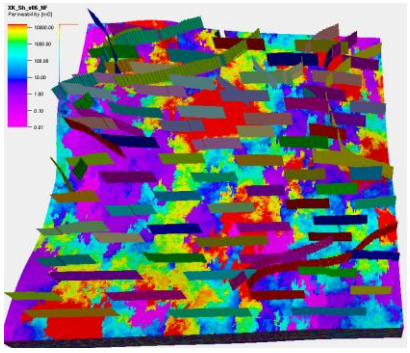

Figure 34. Static Modeling – Full-field model with sub-seismic cero degrees Faults and Structural framework faults

In Figure 35, AoR for three different cases are presented.

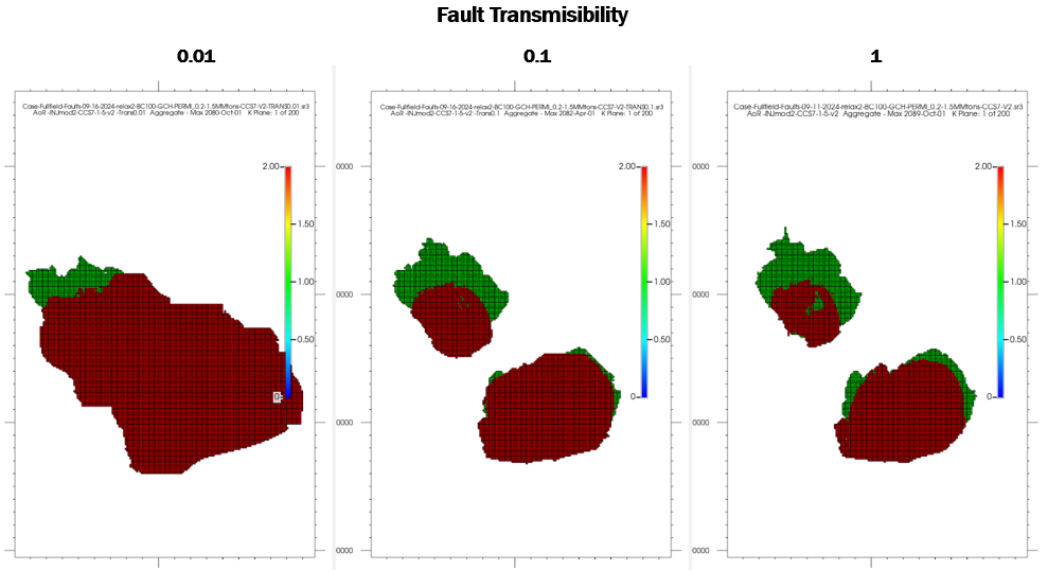

Figure 35. AoR – Full-field model – sensitivity analysis to fault's transmissibility – CO2 Sat (in green) and pressure front (in red)

Figure 35 shows that values of sub-seismic transmissibility equal to or higher than 0.1 do not alter considerably the shape of the AoR. There is a small pressure front difference, but changes in the AoR are negligible with fault transmissibility changes from 0.1 to 1. For reference, our characterization work suggested that realistic sub-seismic faults in this area would have a transmissibility higher than 0.1. Considerable variations of the AoR are observed when faults' transmissibility values close to 0.01 are used. To understand in more detail the main differences in this case, CO_2 saturation and pressure front areas were also calculated separately.

In Figure 36, CO_2 saturation for the three cases is presented for analysis. It can be observed that the CO_2 saturation plume has a minimal change when faults with low transmissibility are included. There are some differences in the shape of the CO_2 plume, where CO_2 follows the orientation of the faults, meanwhile, the shape and size remain similar in all the cases.

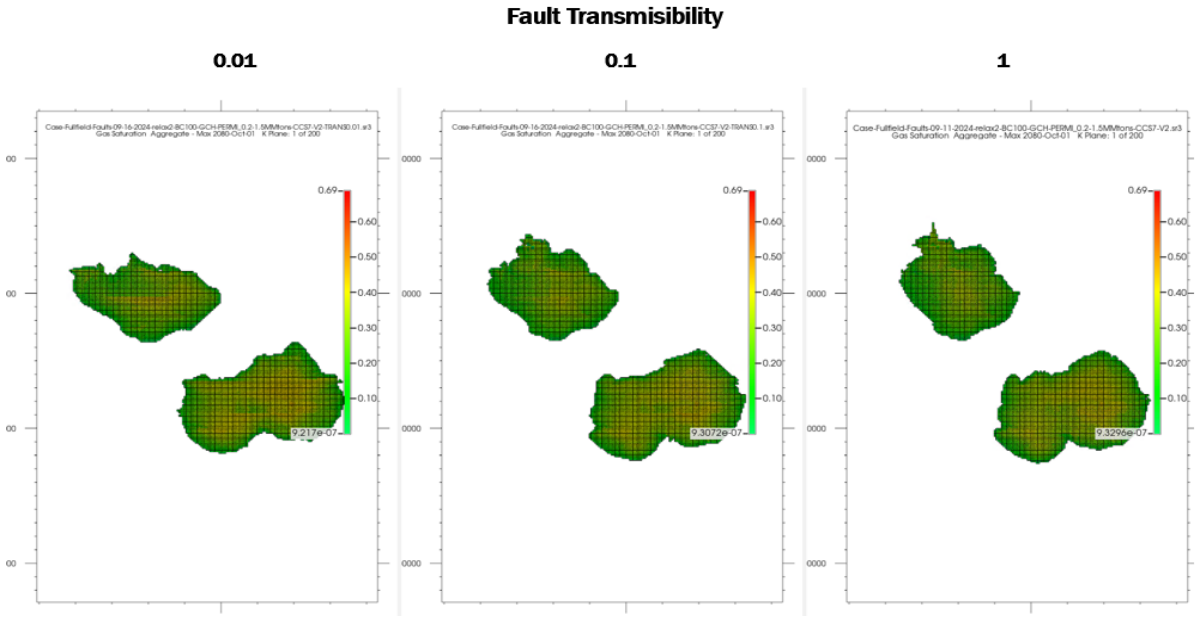

Figure 36. CO_2 Saturation – Full-field model – sensitivity analysis to fault´s transmissibility

A cross-section in one of the injection wells (Well-A) for the three cases is also presented in Figure 37. The objective of this cross-section is to determine if there are relevant vertical CO_2 migration differences when the sub-seismic faults are present. As a result, the CO_2 plume remains similar even in the 0.01 transmissibility value. No additional migration in the vertical axes was observed when sub-seismic faults with very low transmissibility were used.

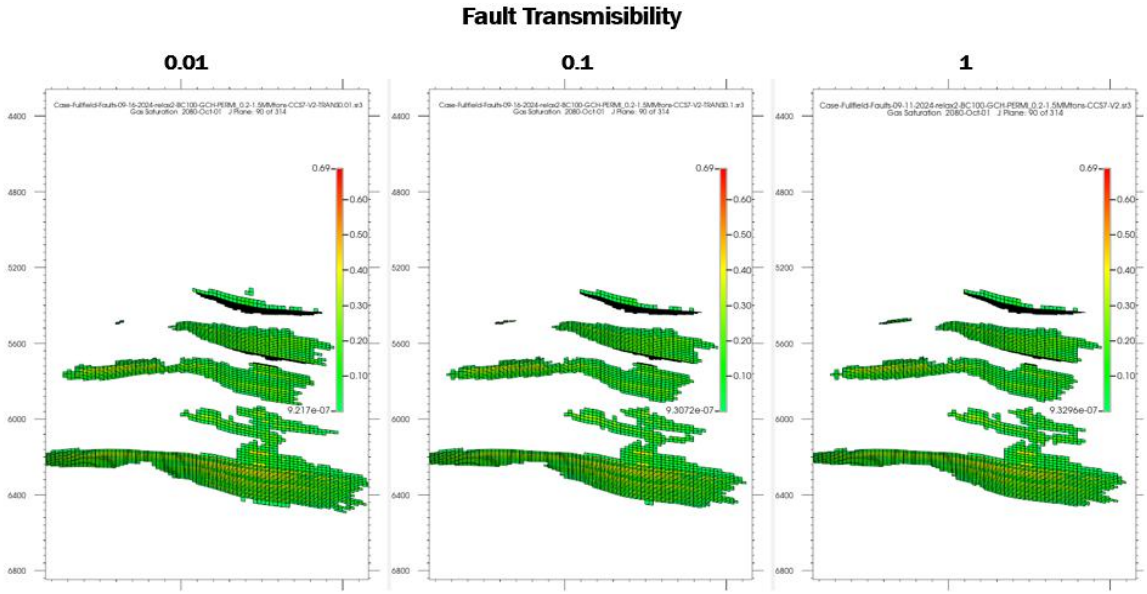

Figure 37. CO_2 Saturation cross section of well-A – Full-field model – sensitivity analysis to fault´s transmissibility

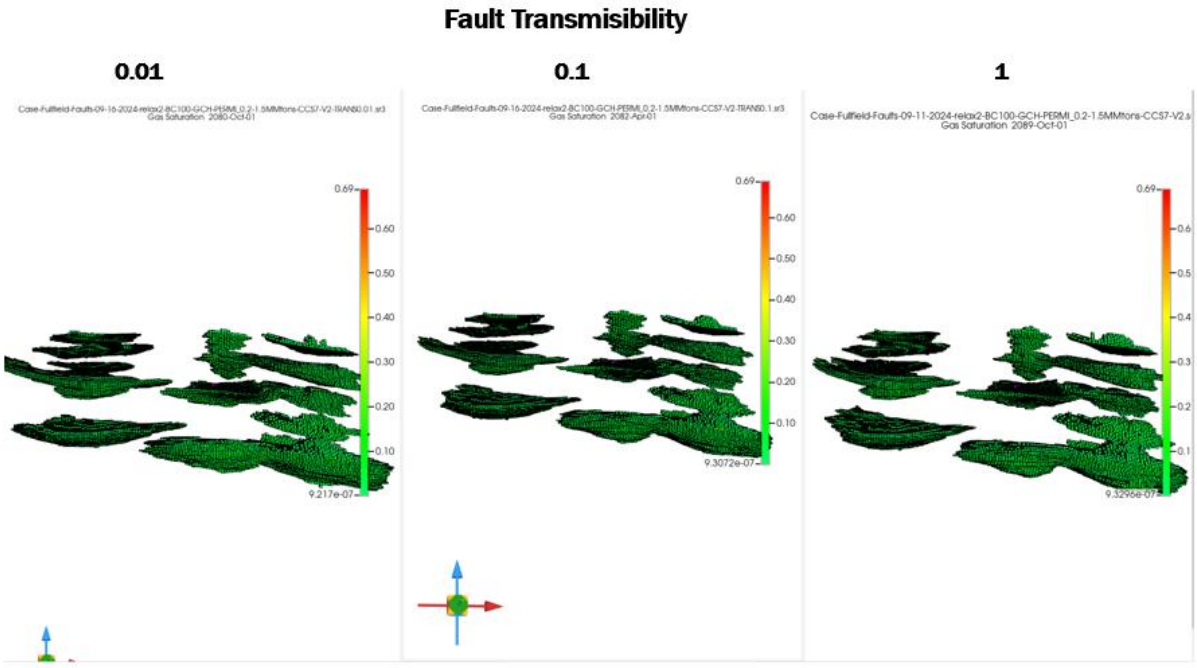

Figure 38. CO_2 Saturation 3D view in the NW-Se direction including the three (3) injection wells – Full-field model – sensitivity analysis to fault´s transmissibility

Figure 38 also shows that CO_2 doesn't migrate from one interval to another, even though, the layers between the injection zones are not real seals. No need of regional sealing formations are required to avoid vertical migration of the CO_2.

In Figures 39-41, pressure front for the three cases were generated. The main change is observed in pressure front for the model with values in the order of 0.01 for fault transmissibility. Similar pressure fronts were obtained for the cases with faults with 0.1 transmissibility and the model with no faults. The main difference in the AoRs is related to the pressure front. When faults with very low transmissibility (in the order of 0.01) are included, the pressure buildup is higher and pressure front travels further into the model.

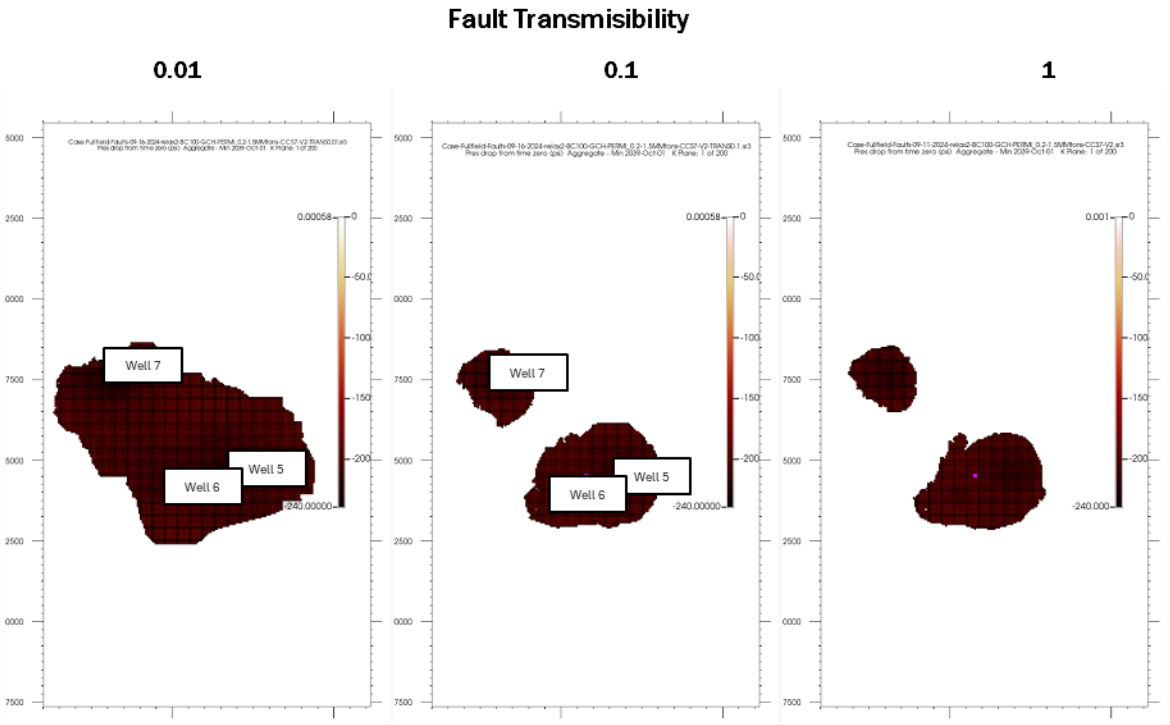

Figure 39. Pressure front – Full-field model – sensitivity analysis to fault´s transmissibility

As it can be observed, in the pressure front cross section, pressure dissipation for the 0.01 transmissibility case is not as fast as it is in the rest of the models. A higher-pressure buildup is observed throughout the model in all the injection zones, which it turns into a bigger final AoR.

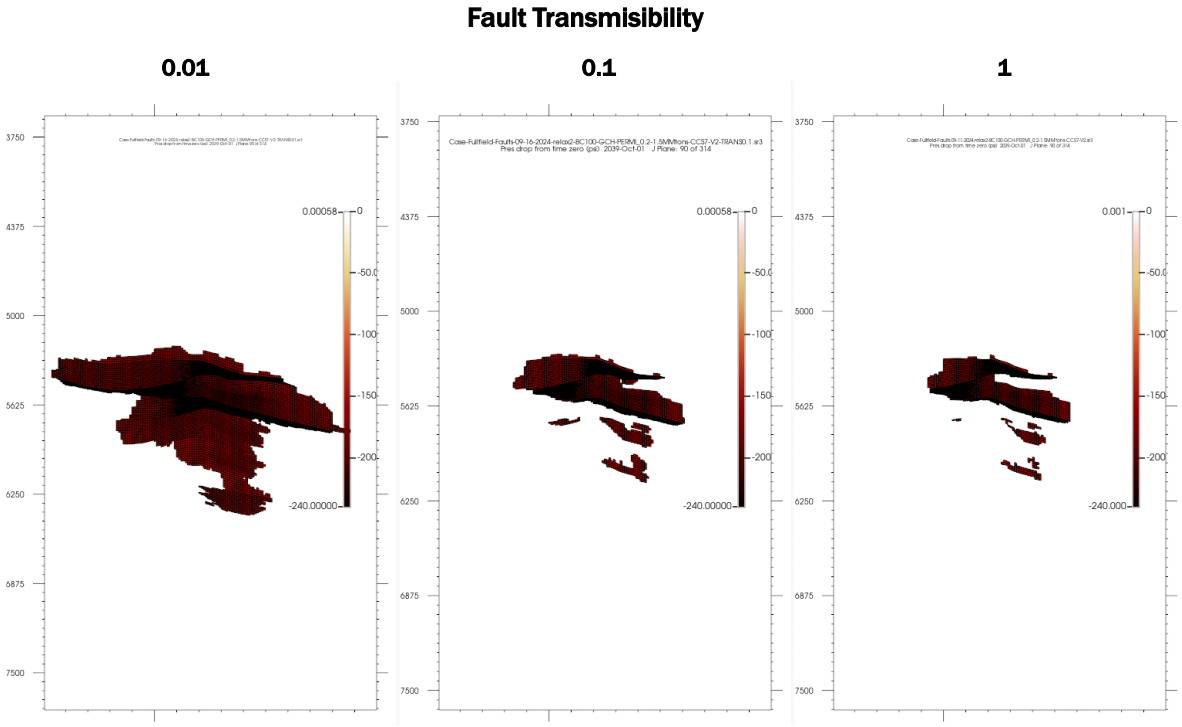

Figure 40. – Pressure front -Cross section at well-A – Full-field model – sensitivity analysis to fault´s transmissibility

In Figures 40 and 41, pressure front shape and AoR for the 0.01 fault transmissibility case are presented, as well as, the permeability associated with that pressure front and AoR.

Pressure front seems to be the main factor affecting AoR shape and size. It is interesting to see that pressure buildup is observed not only in the high permeability injection zones but also in the zones considered as the "buffer zones". These low permeability zones can be considered as pressure dissipation zones even if they have very low permeability values. Pressure propagation is observed in layers with low permeability above and below the injection zones (blue colors in the right of Figure 42) but no CO_2 saturation is observed on those layers. Gas migration is only confined to the higher permeability zones and the low permeability zones act as a barrier to the gas flow in the vertical direction by having higher capillary entry pressure.

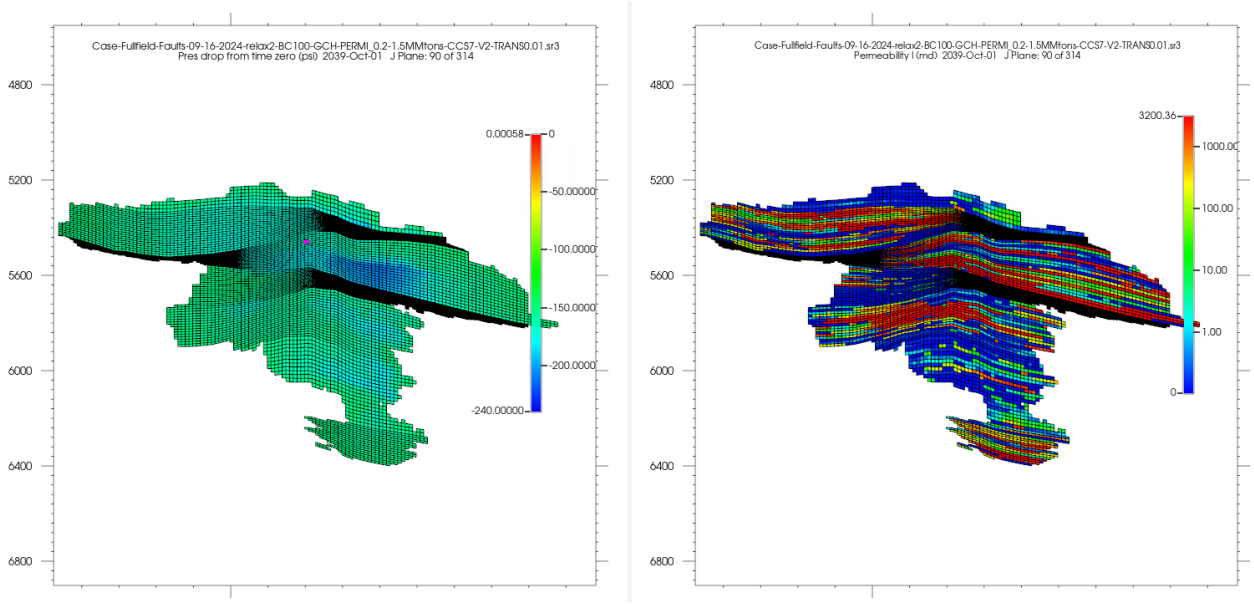

Figure 41. Pressure Front – Full-field model – Case with 0.01 fault´s transmissibility – Pressure front (left) & pressure front plume with permeability values (right)

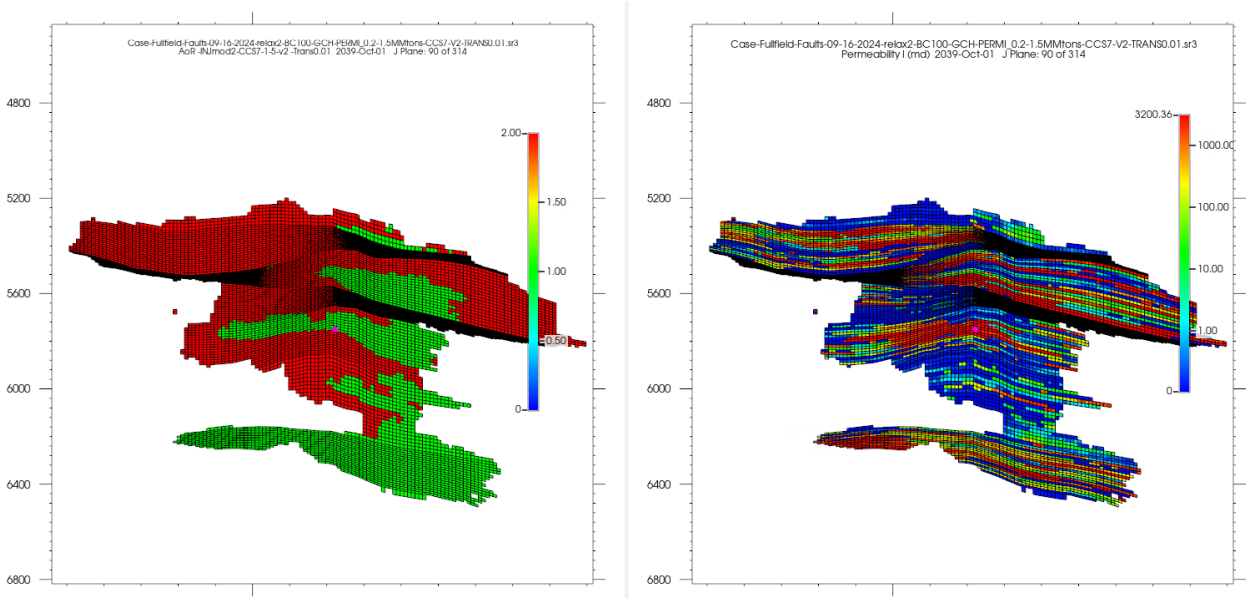

Figure 42. AoR – Full-field model – Case with 0.01 fault´s transmissibility – AoR with pressure front in red and CO_2 plume in green (left) & AoR with permeability values (right)

According to Figures 43 and 44, having a system with thick "buffer zones" could be beneficial for pressure dissipation in the injection formation, and could help to reduce the AoR in projects where the go-area is relatively small.

For the sake of more fully investigating the potential effect of faults on AoR, we ran a final set of models experimenting with fault lengths and transmissibility well beyond the range of realistic sub-seismic faults. This additional sensitivity was related to determine what would be the effect of longer no realistic faults (base case used 3.5 km faults vs. 7km faults length in the sensitivity case) in the AoR. Considering the correlations mentioned in previous sections, faults as long as 7 km could have a throw of 70 m and should be observed in seismic lines interpretation, meanwhile, if for a moment we assume that those faults were not identified in the initial reservoir characterization, the AoR shape and size would be of our interest.

As a result of this sensitivity, the AoR does not change a lot compared with the 3km long faults. The shape of the AoR is different but in general terms, there is no considerable change in both areas.

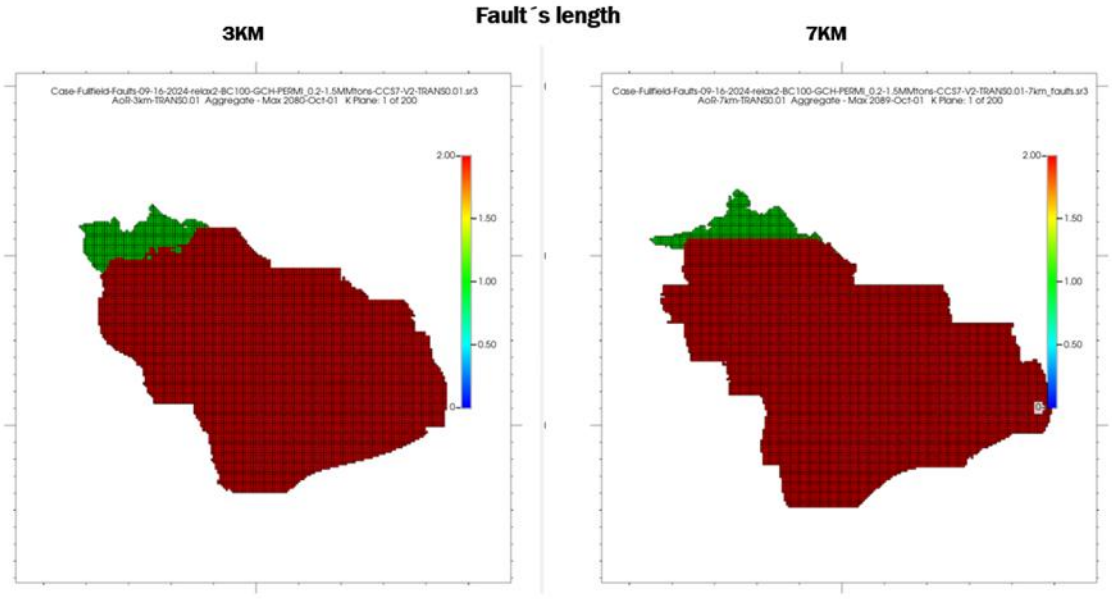

Figure 43. AoR – Full-field model – sensitivity analysis to fault´s length – CO2 Sat (in green) and pressure front (in red)

CO_2 saturation plume at the end of the simulation time for both cases is presented in Figure 44. Some differences in CO_2 saturation are observed. CO_2 saturation against the faults is different but the shape of the plume does not change a lot when the length of the faults is increased from 3.5 to 7 km.

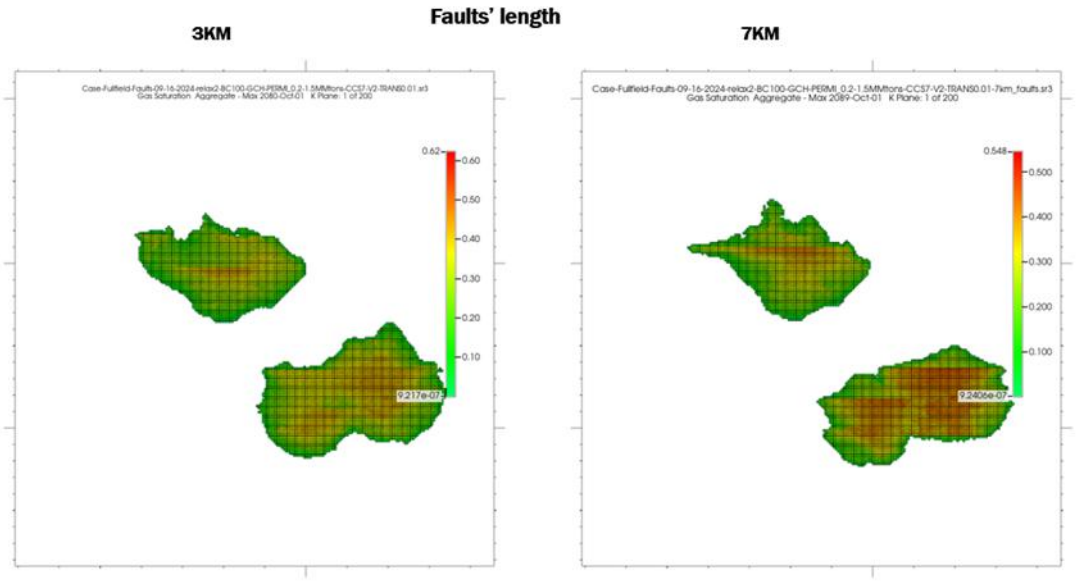

Figure 44. CO_2 Saturation – Full-field model – sensitivity analysis to fault´s length

As a result of this sensitivity, minimal change is observed when the faults´ length is increased from 3.5 km to 7 km. The pressure migrates through the faults and low permeability facies once a minimum pressure is reached and for that reason the final shape of the AoR is similar.

5. CHAPTER V

5.1. DISCUSSION AND IMPLICATIONS FOR CCS

Reservoir characterization is relevant in any CCS project. In this study the effect of sub-seismic faults in the CO_2 migration was evaluated in different scenarios. Sub-seismic fault characterization was predicted using available information on seismic resolution features. This approach can be used in future studies if this information is required.

After including sub seismic faults and overbank permeability variations in the initial models, overbank permeability seems to play a big role in the AoR. The size of the AoR varies with overbank permeabilities, obtaining the largest AoR when overbank permeability is low due to

the low-pressure dissipation within the reservoir. It was also noticed that pressure dissipates in the reservoir even when very low values of overbank permeability are used. On the other hand, CO_2 saturation is mainly limited by high permeability zones and doesn't easily migrate to the low permeability overbank zones. No big effect on AoR size was observed when realistic values of overbank permeability and fault transmissibility were used. For these initial experiments the overbank permeability seems to play a more important role than fault transmissibility in the AoR size.

The results obtained in the first set of experiments were also corroborated in the one single fluid-unit models. For all the geological models used in this stage, when transmissibility values of 0.1 or higher are used (Typical values for sub-seismic faults), no effect on the AoR was observed. Considerably changes in AoR were only observed when fault transmissibility was decreased by at least two orders of magnitude (not realistic in this scenario). In those models, CO_2 saturation follows the channel's direction, but the pressure front follows the fault direction, and bigger AoRs were obtained when faults with cero to ninety degrees direction (perpendicular or oblique to the channel direction) were used. This shows the importance of a good reservoir characterization trying to identify the main possible flow direction of the CO_2 and also identify the main faults direction, that will impact the overall AoR size and shape.

Previous insights obtained in the first stages, were used in the full-field models. As a result of these full-field model dynamic simulations, again realistic values of sub-seismic transmissibility (equal to or higher than 0.1) do not alter considerably the shape of the AoR, which means that these kinds of faults don't play an important role in CO_2 migration and AoR in these scenarios. The area of review shape would only change when transmissibility values are reduced in two orders of magnitude which is not very common in possible sub-seismic faults in this area and geological environment. A considerable reduction in transmissibility (values lower than 0.1) is not common in sub-seismic faults and only might occur if the bed thickness is smaller than the fault's throw, which means that the bed thickness should be less than 30 meters in the sub-seismic faults' cases (Figure 45). In the wells included in this research, most of the injection zones were thicker than 30m and for that reason, the sub-seismic transmissibility values were around 0.1-0.2.

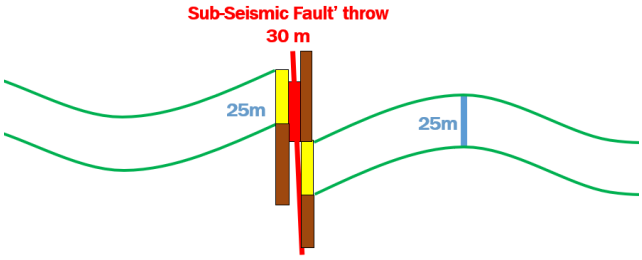

Figure 45. Schematic of low faults' transmissibility value due to thin beds for injection.

Is also important to mention that, one of the limitations of the approach used in this study is that only one value of transmissibility was used for the entire model faults, which in most of the cases is not realistic. Model faults were modeled as a single barrier between two grid blocks, but these faults could be included as grid blocks in the model and a different value of transmissibility could be applied to each of those grids depending on the SGR and transmissibility calculations.

In the case where very low fault transmissibility values were used (0.01), the AoR was considerably bigger and shape was mainly affected by the pressure front; high-pressure buildup was observed not only in the injection zones but also in the above and beneath formations where permeability values were very low. Pressure dissipation was observed throughout the model, converting the low permeability zones into "buffers" for pressure dissipation. On the other hand, CO_2 migration was limited only to the injection zones with high permeability values. This is a first approach proving that the concept of composite confinement systems proposed by (Bump, 2023) is an effective way to store big quantities of CO_2 in zones where no continuous impermeable layers are present.

According to these results, the main take away for the project developers and operators of this project is that they should not be worried about sub-seismic features when developing their projects. They also should know that low permeability zones can act as barriers to CO_2 migration keeping the CO_2 plume within the high permeability zones. Low permeability zones can act as pressure dissipation formations reducing the size of the AoR, which could have a big impact on the economic viability of the project; reducing the proximity to legacy wells and

monitoring strategies costs, keeping the CO_2 and pressure away from preexisting oil and gas fields, reducing cost due to leasing areas acquisition and enabling new areas for CO_2 injection that were not considered suitable for this kind of projects before due to the lack of a regional impermeable seal.

The operator should not worry about sub-seismic features causing unintended lateral migration and they should focus efforts on seismic-scale features characterization and low permeability zones characterization. At the same time, operator should consider that areas with heterogeneous geology with several injection zones without a regional seal can also be used for CO_2 injection purposes and could be store big quantities of CO_2. AoR size and shape simulation is mainly driven by a proper boundary's definition, the further the limits of the boundary, the smallest the pressure front and AoR would be, so a proper boundary definition is crucial when evaluating a project.

6. CHAPTER VI

6.1. CONCLUSIONS AND FUTURE WORK

Every month, several commercial CCS projects are being announced and developed on the Gulf Coast of the USA. Most of these projects will be developed in heterogeneous geology formations as the Miocene formation that was evaluated in this study. Projects are also being placed within oddly-shaped leases and keeping CO_2 within these leases is of main importance. During this study, the role that could play sub-seismic faults and channels that are not easily identified through conventional methods in CO_2 migration within the leasing area was evaluated.

Miocene formation in onshore Texas area is characterized for being heterogeneous reservoirs of unconsolidated fluvio-deltaic depositional systems with the presence of faults generally perpendicular to the direction of the channel flow complexes. Big faults and flow channels are well identified through seismic lines interpretation, well logs, cores, etc., meanwhile, sub-seismic faults and channels are not easily identified through conventional methods. The effect

of these sub-seismic features in the fluid flow behavior of CO_2 plume in potential CCS storage projects was analyzed in this research. Possible unintended lateral migration of the CO_2 beyond the leasing area or unintended high-pressure fronts due to those sub-seismic features was the main problem to be addressed in this study.

The first step to address this problem was to characterize the faults, channels and rock properties of the injection zones in the area of interest. A methodology to predict sub-seismic faults and channel characteristics using available information on seismic resolution features was developed. For channel and fault characterization, seismic amplitudes extractions interpretation, 2D-3D seismic lines, field reports, as well as, a literature review of previous correlations obtained by different authors were used to determine characteristics that were used to build the first static models.

Another important sub-seismic fault' characteristic addressed during this study was the fault seal capacity. Several authors have worked on this subject before and an extensive literature review was performed to determine the best approach to determine the seal capacity of sub-seismic faults. A methodology applied to a real well log data of a well located in the area of interest was implemented. This methodology combines SGR developed by (G. Yielding, B. Freeman, And D. T., 1997) with the transmissibility multiplier approach developed by (Manzocchi et al., 1999) to predict transmissibility values. As a result, transmissibility values that range between 0.1-0.2 for the sub-seismic faults with a throw lower than 30 meters were obtained.

Saturation functions in CO_2 injection formations are also very important to determine storage capacity and fluid flow behavior during site characterization projects, meanwhile, this information is usually not available due to the lack of experimental studies in areas away from what historically has been the interest for conventional oil and gas reservoirs. In the GOM, CO_2 injection projects are being located away from oil and gas fields, legacy wells, and any potential leakage path. For that reason, capillary pressure and relative permeability curves are not commonly available. In this research, a methodology to obtain capillary pressure and relative permeability curves was developed. Results obtained with this methodology were compared with real core data and good results were achieved. If no information on these curves is available

in the area of interest, this methodology can be used to generate them. Reservoir engineers can use the proposed workflow to obtain a first set of relative permeability curves and capillary pressure for the dynamic modeling if no other information is available.

After including channels, sub-seismic faults and petrophysical properties in the static and dynamic models, several sensitivity cases were run to evaluate the effect of them in the AoR size. As result, no considerable effect was observed in CO_2 lateral migration or AoR shape and size of the models when sub-seismic faults with realistic characteristics were included. AoR remained constant in area after these sub-seismic features were included even when the faults characteristics used were modified to the upper limits to try to make the model fail.

Several sensitivities were evaluated to determine if unintended lateral migration could be a problem in this kind of scenario. As a result of these sensitivities, it was observed that the sub-seismic faults only would play a big role if their transmissibility is in the order of 0.01 or lower (not typical values for sub-seismic faults in the area of interest). In those cases, the size and shape of the AoR will be much bigger than the model without faults. AoR and CO_2 plumes will also be affected by the direction of the faults with respect to the flow channels. Faults perpendicular or oblique to the flow channels will play a big role in the lateral migration of the CO_2 and pressure dissipation. In contrast, faults parallel or semi-parallel to the flow channels won't play any role in CO_2 migration.

In any dynamic model, lease and project boundaries are of main importance. How big your boundaries are beyond the leasing area and how those limits are defined by the operator would make a big difference in the final AoR size and shape.

In full-field models, CO_2 injection was performed in different intervals within Miocene formation. As a result, CO_2 migration was limited to the zones with high permeability and there was no migration between injection zones when sub-seismic faults with typical characteristics were included. Faults played a role in AoR size only when very low transmissibility values were used. Even though low permeability zones above and beneath the injection zones are not considered to be regional seals or impermeable formations, they acted as a barrier to CO_2 migration; This is a demonstration that the composite confinement system concept could safely retain big quantities of CO_2 within the injection zones. Additionally, is also important to point

out that those low permeability zones acted as pressure sinks. Pressure increase was observed throughout the model and having additional zones between the injection zones helped pressure to be dissipated on those zones and AoR to be smaller than expected.

Uncertainty is always a fact, and in any reservoir characterization and dynamic simulation, is a constant. Any good research generates as many questions as it answers and this has generated several. Future work could be focused on getting a better reservoir and fluid characterization as well as performing additional sensitivity analysis, choosing additional parameters that were used in the simulation model to perform the sensitivity analysis in the full-filed model. Properties such as compressibility, kv/kh, boundaries extension, residual gas saturation, and permeability multiplier can be used as sensitivity parameters. Evaluating unintended CO_2 migration using these additional sensitivities could lead to evaluate extra costs caused by additional leasing area, increase in monitoring plans, and legacy well remediation, among others. Evaluation of different strategies such as drilling pressure relief wells, perforation of additional intervals, and acquiring more leasing area could also be considered to reduce the AoR in case the leasing area is smaller than expected AoR.

As a general conclusion, this study showed that predicting CO_2 plume migration is both important and fraught with considerably subsurface uncertainty, but sub-seismic faults doesn't seem to be something to worry about, at least not in this setting.

7. APPENDIX

7.1. APPENDIX I

Matrix results for the realistic but flexible models for CO_2 saturation and pressure front are presented in Figures 46 through 53. For the continuous narrow geometry geological model, Figures 46 and 47 illustrate the results obtained:

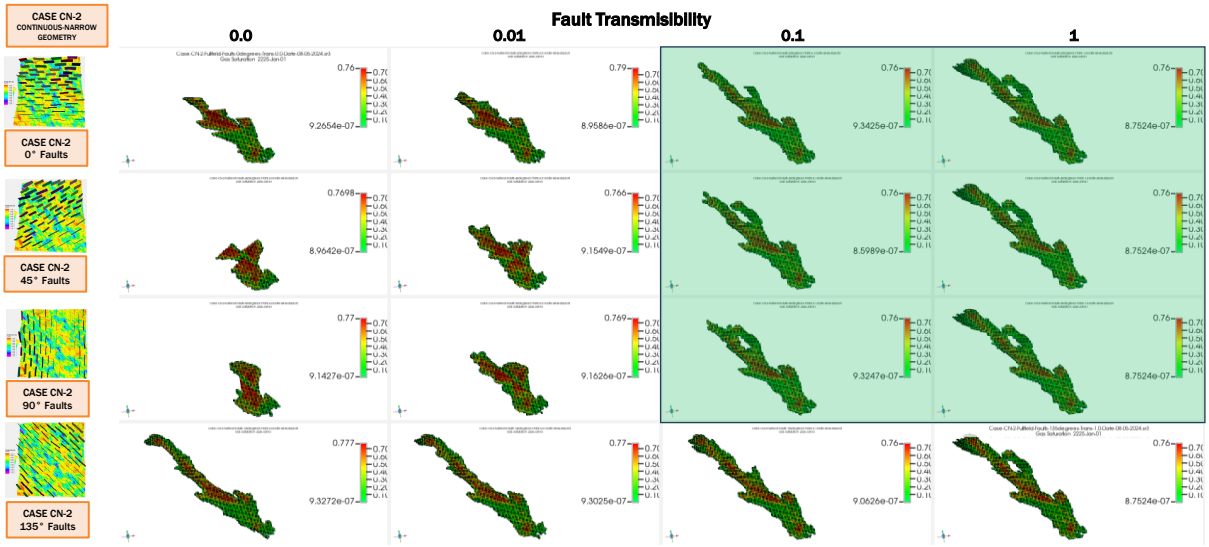

Figure 46. Realistic but flexible model –continuous narrow geometry geological model – CO_2 Saturation map

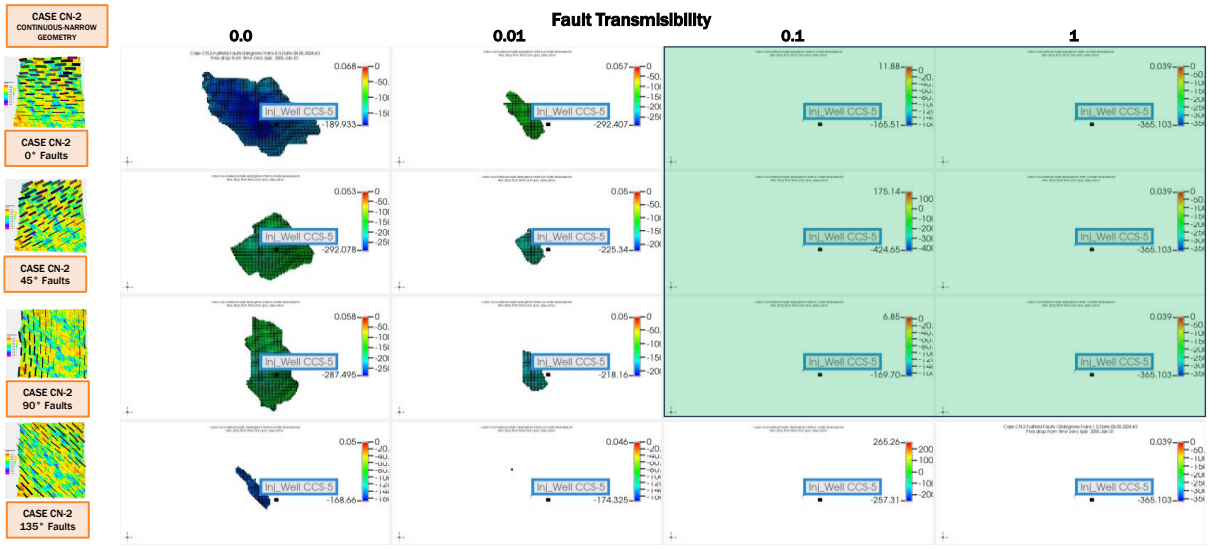

Figure 47. Realistic but flexible model –continuous narrow geometry geological model – Pressure front map

For the discontinuous narrow geometry geological model, Figure 48 illustrates the results obtained:

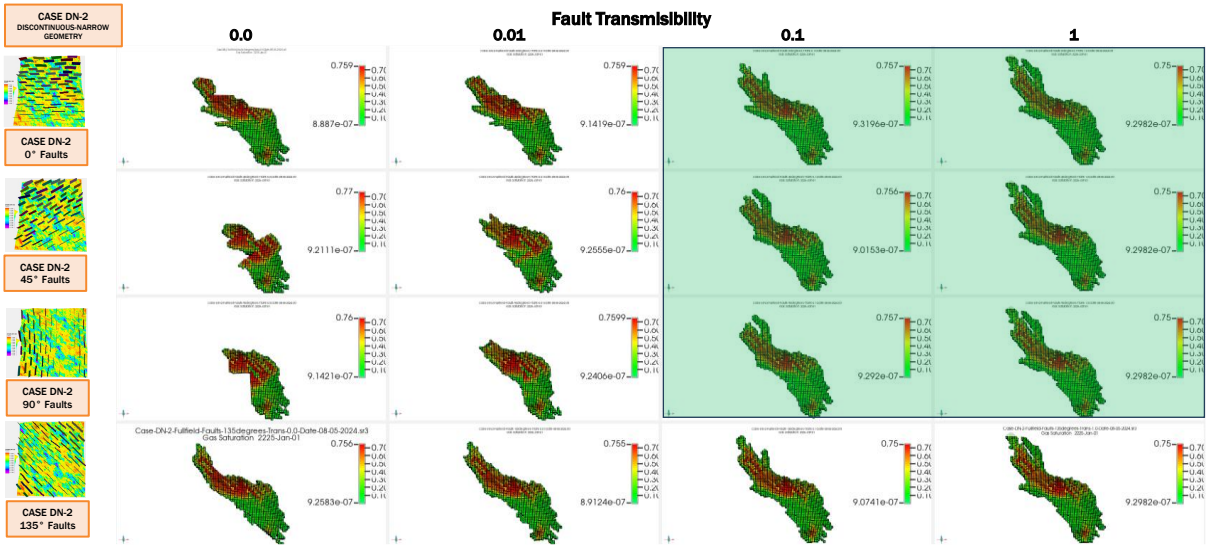

Figure 48. Realistic but flexible model –Discontinuous narrow geometry geological model – CO_2 Saturation map

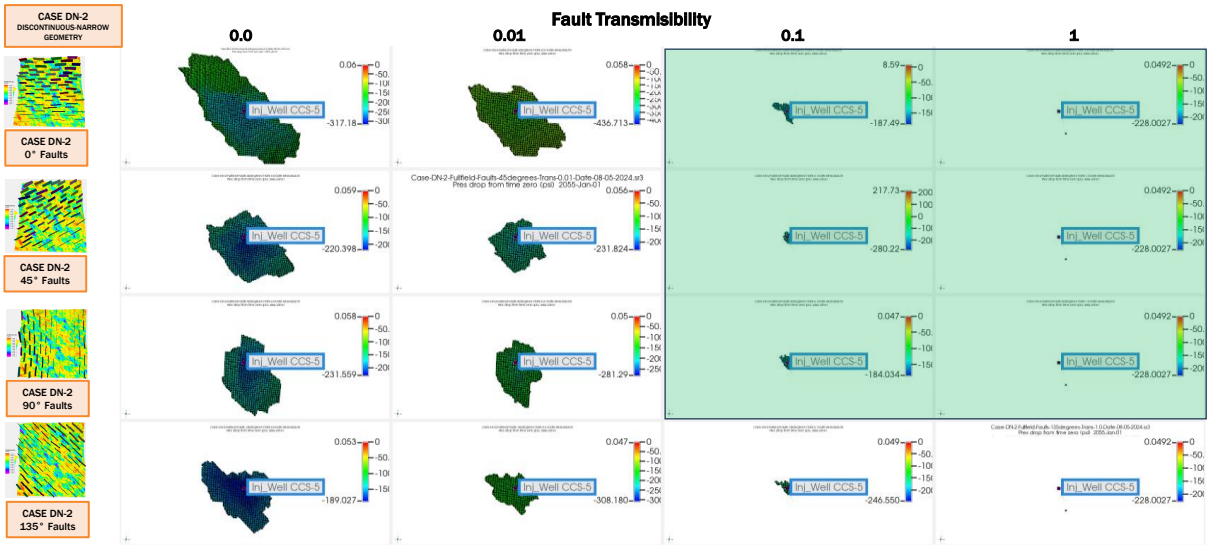

Figure 49. Realistic but flexible model –Discontinuous narrow geometry geological model – Pressure front map

For the continuous wide geometry geological model, Figures 50 and 51 illustrate the results obtained:

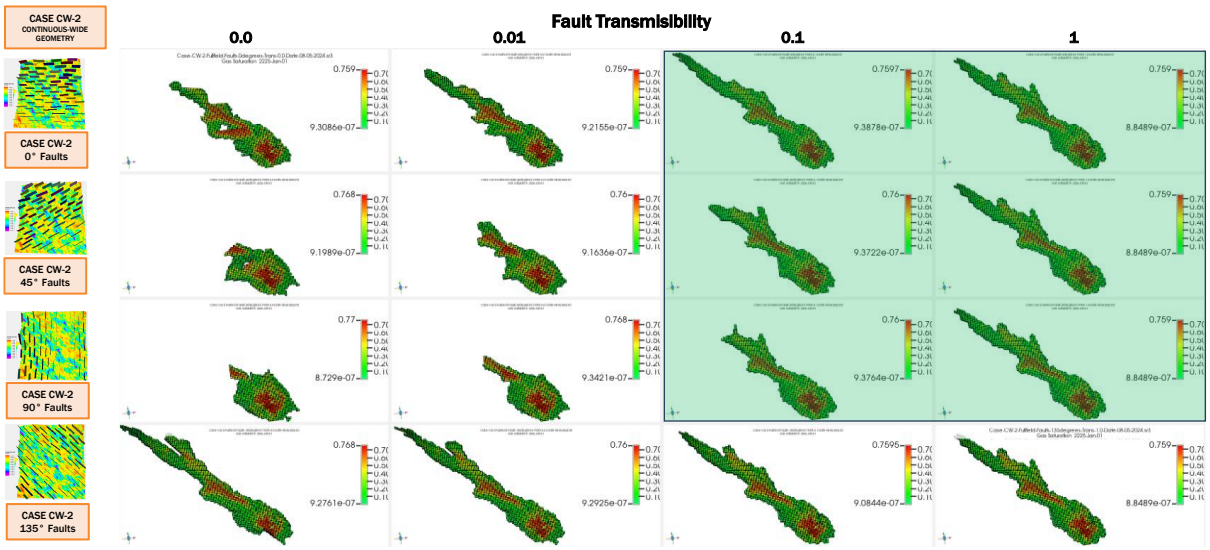

Figure 50. Realistic but flexible model –Continuous wide geometry geological model – CO_2 Saturation map

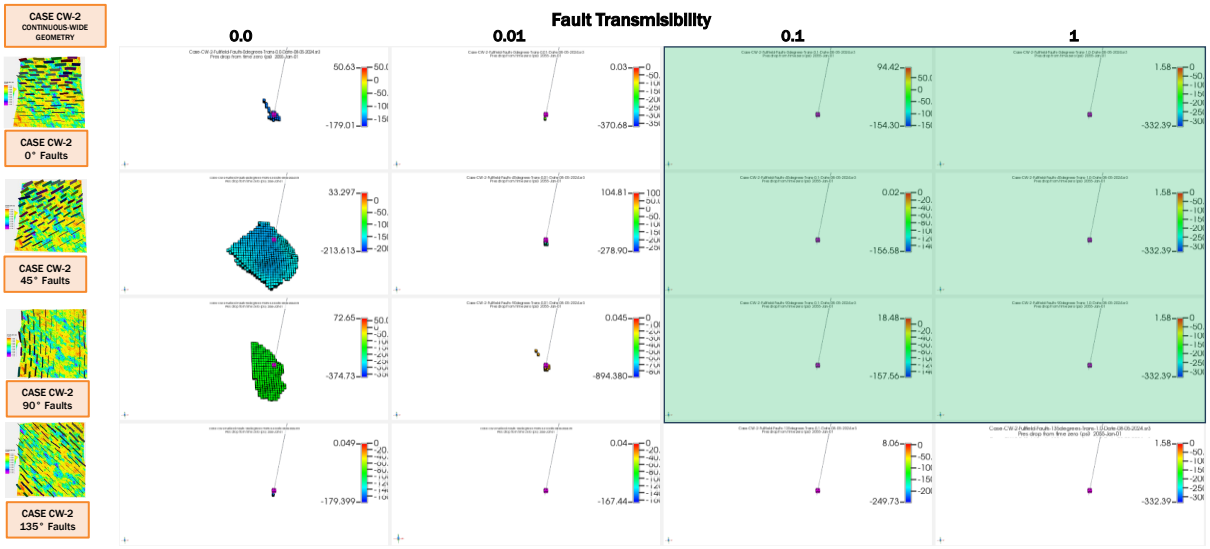

Figure 51. AoR – Realistic but flexible model – Continuous wide geometry geological model – Pressure front map

For the discontinuous wide geometry geological model, Figures 52 and 53 illustrate the results obtained:

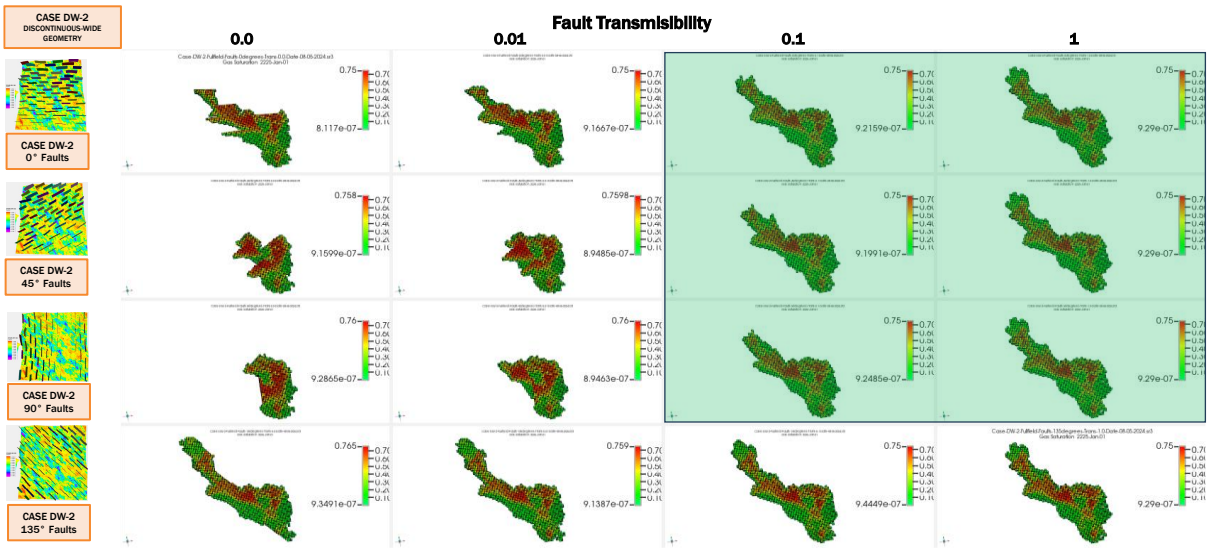

Figure 52. Realistic but flexible model –Discontinuous wide geometry geological model – CO_2 Saturation map

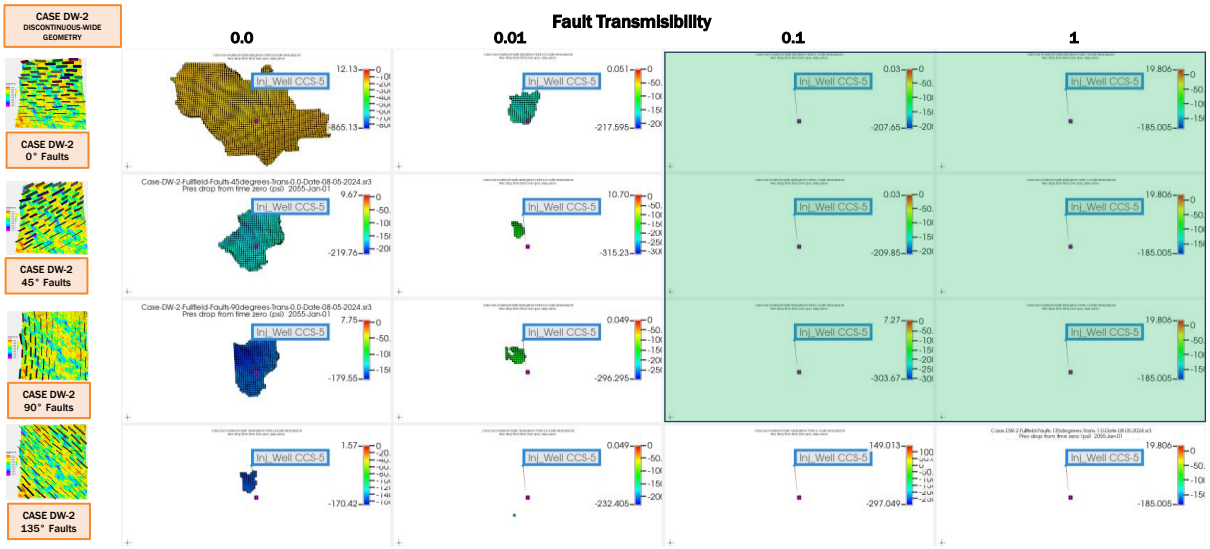

Figure 53. Realistic but flexible model – Discontinuous wide geometry geological model – Pressure front map

7.2. APPENDIX II

Figure 54 presents a schematic explanation of the boundary area. This area should be defined by the operator based on the available geological information and the knowledge of the area of interest. If the boundary area is bigger than the model area, open boundary conditions could be established in the dynamic model and volume modifiers and transmissibility multipliers should be applied to the outer cells of the model. An explanation of recommended values to be used as volume modifiers and transmissibility multipliers was presented by (Hosseini et al., 2024).

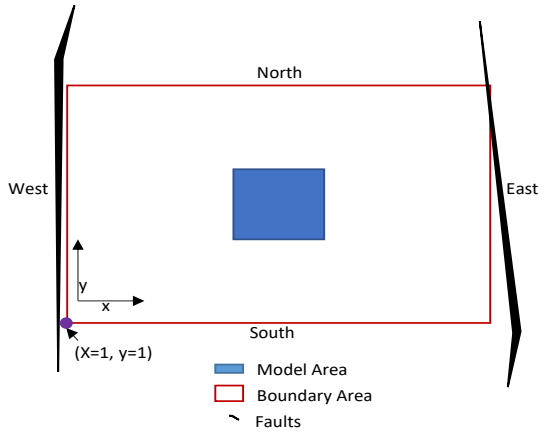

Figure 54. top view – Open boundary concept explanation

Properly including these parameters in CMG Software is very important because it will make a big difference for the AoR and pressure front. The following lines present a workflow of how to include open boundary conditions in the .dat file in CMG Software. In this case is assumed that the boundaries in all directions are at the same distance, but if they are not, the values of VOLMOD, TRANSI, and TRANLI for each side of the model should change accordingly. More information on how to use these keywords can be found in the User's Manual of GEM-CMG Software.

```
VOLMOD CON          1
*MOD
  1:1 1:285 1:200   = 100 **West
  2:287 1:1 1:200   = 100 **South
  288:288 1:285 1:200   = 100 **East
  2:287 285:285 1:200   = 100 **North
```

```
TRANSI *MATRIX *IJK
 2:287 1:1 1:200   100  **South
 1:1 1:285 1:200   0.0094 **West  This value corresponds to 1/(volmod+1)
 2:287 285:285 1:200    100 **North
TRANLI *MATRIX *IJK
 288:288 1:285 1:200   0.0094  **East
TRANSJ *MATRIX *IJK
 1:1 1:285 1:200   100 **West
 288:288 1:285 1:200   100 **East
 2:287 1:1 1:200   0.0094 **South
TRANLJ *MATRIX *IJK
  2:287 285:285 1:200   0.0094 **North
 TRANSK *MATRIX *IJK
 1:1 1:285 1:200   100 **West
 2:287 1:1 1:200   100 **South
 288:288 1:285 1:200   100 **East
 2:287 285:285 1:200   100 **North
```

8. REFERENCES

A. D. Reynolds. (1999). Dimensions of Paralic Sandstone Bodies. *AAPG Bulletin*, *83 (1999)*. https://doi.org/10.1306/00AA9A48-1730-11D7-8645000102C1865D

Alfi, M., & Hosseini, S. A. (2016). Integration of reservoir simulation, history matching, and 4D seismic for CO_2-EOR and storage at Cranfield, Mississippi, USA. *Fuel*, *175*, 116–128. https://doi.org/10.1016/j.fuel.2016.02.032

Armstrong, C., Mohrig, D., Hess, T., George, T., & Straub, K. M. (2014). Influence of growth faults on coastal fluvial systems: Examples from the late Miocene to Recent Mississippi River Delta. *Sedimentary Geology*, *301*, 120–132. https://doi.org/10.1016/j.sedgeo.2013.06.010

Baker, R. (2015). 8-Special Core Analysis -Rock-Fluid Interactions. In R. Baker, *Practical Reservoir Engineering and Characterization* (p. 521). Calgary, Canada: Gulf Professional Publishing.

Berg, R. (1975). Capillary pressures in stratigraphic traps. *AAPG Bull. 59*, 939-956.

Brooks, R. (1965). *Hydraulic Properties of porous media.* Colorado State University.

Brooks, R. H., & Corey, A. T. (n.d.). *HYDRAULIC PROPERTIES OF POROUS MEDIA*.

Bruno, M. e. (2014). Characterization of Pliocene and Miocene formations in the Wilmington Graben, Offshore Los Angeles, for large scale geologic storage of CO_2. *Energy Procedia*, 4897-4917.

Bump, A. (2023). Composite confining systems: Rethinking geologic seals for permanent CO_2 sequestration. *International Journal of Greenhouse Gas Control*, 12.

Bureau of Economic Geology, Treviño, R. H., Meckel, T. A., & Bureau of Economic Geology. (2017). *Geological CO_2 Sequestration Atlas of Miocene Strata, Offshore*

Texas State Waters (Report of Investigations) [Report of Investigations]. The University of Texas at Austin, Bureau of Economic Geology. https://doi.org/10.23867/RI0283D

Clarke, S. M., Burley, S. D., & Williams, G. D. (2005). A three-dimensional approach to fault seal analysis: Fault-block juxtaposition & argillaceous smear modelling. *Basin Research*, *17*(2), 269–288. https://doi.org/10.1111/j.1365-2117.2005.00263.x

Delshad, M., Kong, X., Tavakoli, R., Hosseini, S. A., & Wheeler, M. F. (2013). Modeling and simulation of carbon sequestration at Cranfield incorporating new physical models. *International Journal of Greenhouse Gas Control*, *18*, 463–473. https://doi.org/10.1016/j.ijggc.2013.03.019

EIA. (2022, 12 01). *EIA*. Retrieved from EIA: https://www.eia.gov/environment/emissions/carbon/

El Sharawy, M. S., & Gaafar, G. R. (2019). Impacts of petrophysical properties of sandstone reservoirs on their irreducible water saturation: Implication and prediction. *Journal of African Earth Sciences*, *156*, 118–132. https://doi.org/10.1016/j.jafrearsci.2019.04.016

EPA. (2024, 01 30). *EPA*. Retrieved from Environmental Protection Agency: https://ghgdata.epa.gov/ghgp/main

European Environment Agency. (2014, 10 31). *European Environment Agency*. Retrieved from EEA: https://www.eea.europa.eu/data-and-maps/figures/correlation-of-per-capita-energy

Fisher, Q. J., Haneef, J., Grattoni, C. A., Allshorn, S., & Lorinczi, P. (2018). Permeability of fault rocks in siliciclastic reservoirs: Recent advances. *Marine and Petroleum Geology*, *91*, 29–42. https://doi.org/10.1016/j.marpetgeo.2017.12.019

Galloway, W. e. (2000). Cenozoic depositional history of the Gulf of Mexico basin. *AAPG Bulletin*, 1743-1774.

GAO. (2022). *Decarbonization. Status, Challenges, and Policy Options for Carbon Capture, Utilization, and Storage.* Washington, DC: US Government Accountability Office.

G. Yielding, B. Freeman, And D. T. (1997). Quantitative Fault Seal Prediction. *AAPG Bulletin*, *81 (1997)*. https://doi.org/10.1306/522B498D-1727-11D7-8645000102C1865D

Ghomian, Y., Pope, G. A., & Sepehrnoori, K. (2008). Reservoir simulation of CO_2 sequestration pilot in Frio brine formation, USA Gulf Coast. *Energy*, *33*(7), 1055–1067. https://doi.org/10.1016/j.energy.2008.02.011

Gibling, M. R. (2006). Width and Thickness of Fluvial Channel Bodies and Valley Fills in the Geological Record: A Literature Compilation and Classification. *Journal of Sedimentary Research*, *76*(5), 731–770. https://doi.org/10.2110/jsr.2006.060

Gillespie, P., Casini, G., Iben, H., & O'Brien, J. F. (2018). Simulation of subseismic joint and fault networks using a heuristic mechanical model. *Geological Society, London, Special Publications*, *459*(1), 177–190. https://doi.org/10.1144/SP459.6

Gutiérrez Paredes, H. C., Catuneanu, O., & Hernández Romano, U. (2018). Controls on the quality of Miocene reservoirs, southern Gulf of Mexico. *Journal of South American Earth Sciences*, *81*, 45–65. https://doi.org/10.1016/j.jsames.2017.10.007

Herve Jourde,1 Eric A. Flodin,2 Ati. (2002). Computing permeability of fault zones in eolian sandstone from outcrop measurements. *AAPG Bulletin*, *86*. https://doi.org/10.1306/61EEDC4C-173E-11D7-8645000102C1865D

Holtz, M. H. (n.d.). *Petrophysical Characterization of Permian Shallow-Water Dolostone*.

Hosseini, S. A., Ershadnia, R., Lun, L., Morgan, S., Bennett, M., Skrivanos, C., Li, B., Soltanian, M. R., Pawar, R., & Hovorka, S. D. (2024). Dynamic modeling of geological carbon storage in aquifers – workflows and practices. *International Journal of Greenhouse Gas Control*, *138*, 104235. https://doi.org/10.1016/j.ijggc.2024.104235

Hosseini, S. A., Lashgari, H., Choi, J. W., Nicot, J.-P., Lu, J., & Hovorka, S. D. (2013). Static and dynamic reservoir modeling for geological CO_2 sequestration at Cranfield, Mississippi, U.S.A. *International Journal of Greenhouse Gas Control*, *18*, 449–462. https://doi.org/10.1016/j.ijggc.2012.11.009

IEA. (2023, 03 24). *CCUS Project Explorer*. Retrieved from IEA: https://www.iea.org/data-and-statistics/data-tools/ccus-projects-explorer

IPCC. (2005). *Carbon Dioxide Capture and Storage.* New York: Intergovernmental Panel on Climate Change.

IPCC. (2019). *Global warming of 1.5C.* Intergovernmental Panel on Climate Change.

John S. Bridge2 And Robert S. Tye3. (2000). Interpreting the Dimensions of Ancient Fluvial Channel Bars, Channels, and Channel Belts from Wireline-Logs and Cores. *AAPG Bulletin*, *84*. https://doi.org/10.1306/A9673C84-1738-11D7-8645000102C1865D

Kabir, M. e. (2023). Climate change due to increasing concentration of carbon dioxide and its impacts on environment in 21st century: a mini review. *Journal of King Saud University*, 7.

Kozak, J. A., Ahuja, L. R., Ma, L., & Green, T. R. (2005). Scaling and Estimation of Evaporation and Transpiration of Water across Soil Textures. *Vadose Zone Journal*, *4*(2), 418–427. https://doi.org/10.2136/vzj2004.0119

Krishnamurthy, P. G., DiCarlo, D., & Meckel, T. (2022). Geologic Heterogeneity Controls on Trapping and Migration of CO 2. *Geophysical Research Letters*, *49*(16), e2022GL099104. https://doi.org/10.1029/2022GL099104

Larue, D. K., Allen, J., Beeson, D., & Robbins, J. (2023). Fluvial reservoir architecture, directional heterogeneity and continuity, recognizing incised valley fills, and the case for nodal avulsion on a distributive fluvial system: Kern River field, California. *AAPG Bulletin*, *107*(3), 477–513. https://doi.org/10.1306/09232220163

Lowry, P., & Jacobsen, T. (1993). Sedimentological and reservoir characteristics of a fluvial-dominated delta-front sequence: Ferron Sandstone Member (Turonian), East-central Utah, USA. *Geological Society, London, Special Publications*, *69*(1), 81–103. https://doi.org/10.1144/GSL.SP.1993.069.01.05

Meckel, T. (2010). *Capillary seals for trapping carbon dioxide (CO_2) in undergroundreservoirs.* Cambridge, UK, ISBN 978 1845697976: Woodhead Publishing Limited.

Meckel, T. (2015). *International Journal of Greenhouse Gas Control*, 85-96.

Maerten, L., Gillespie, P., & Daniel, J.-M. (2006). Three-dimensional geomechanical modeling for constraint of subseismic fault simulation. *AAPG Bulletin*, *90*(9), 1337–1358. https://doi.org/10.1306/03130605148

Manzocchi, T., Walsh, J. J., Nell, P., & Yielding, G. (1999). Fault transmissibility multipliers for flow simulation models. *Petroleum Geoscience*, *5*(1), 53–63. https://doi.org/10.1144/petgeo.5.1.53

Miocic, J. M., Johnson, G., & Bond, C. E. (2019). *Uncertainty in fault seal parameters: Implications for CO₂ columnheight retention and storage*

capacity in geological CO₂ storageprojects [Preprint]. The evolving Earth surface/Rock deformation, geomorphology, morphotectonics, and paleoseismology/Structural geology. https://doi.org/10.5194/se-2019-55

Ni, H., Bakhshian, S., & Meckel, T. A. (2023). Effects of grain size and small-scale bedform architecture on CO_2 saturation from buoyancy-driven flow. *Scientific Reports*, *13*(1), 2474. https://doi.org/10.1038/s41598-023-29360-y

Nicol, A., Seebeck, H., Field, B., McNamara, D., Childs, C., Craig, J., & Rolland, A. (2017). Fault Permeability and CO_2 Storage. *Energy Procedia*, *114*, 3229–3236. https://doi.org/10.1016/j.egypro.2017.03.1454

Nicot, J.-P., Oldenburg, C. M., Bryant, S. L., & Hovorka, S. D. (2009). Pressure perturbations from geologic carbon sequestration: Area-of-review boundaries and borehole leakage driving forces. *Energy Procedia*, *1*(1), 47–54. https://doi.org/10.1016/j.egypro.2009.01.009

NPC. (2021). *Meeting the Dual Challenge.* National Petroleum Council.

NPMS. (2024, 1 11). *National Pipeline Mapping System*. Retrieved from National Pipeline Mapping System: https://www.npms.phmsa.dot.gov/Documents/NPMS_CO_2_Pipelines_Map.pdf

Olariu, C., & Bhattacharya, J. P. (2006). Terminal Distributary Channels and Delta Front Architecture of River-Dominated Delta Systems. *Journal of Sedimentary Research*, *76*(2), 212–233. https://doi.org/10.2110/jsr.2006.026

Olariu, M. I., DeAngelo, M., Dunlap, D., & Treviño, R. H. (2019). High frequency (4th order) sequence stratigraphy of Early Miocene deltaic shorelines, offshore Texas and

Louisiana. *Marine and Petroleum Geology*, *110*, 575–586. https://doi.org/10.1016/j.marpetgeo.2019.07.040

Olson, J. E., Laubach, S. E., & Lander, R. H. (2009). Natural fracture characterization in tight gas sandstones: Integrating mechanics and diagenesis. *AAPG Bulletin*, *93*(11), 1535–1549. https://doi.org/10.1306/08110909100

Pei, Y., Paton, D. A., Knipe, R. J., & Wu, K. (2015). A review of fault sealing behaviour and its evaluation in siliciclastic rocks. *Earth-Science Reviews*, *150*, 121–138. https://doi.org/10.1016/j.earscirev.2015.07.011

Pickering, G., Bull, J. M., & Sanderson, D. J. (1996). Scaling of fault displacements and implications for the estimation of sub-seismic strain. *Geological Society, London, Special Publications*, *99*(1), 11–26. https://doi.org/10.1144/GSL.SP.1996.099.01.03

Pickering, G. e. (1996). Scaling of fault displacements and implications for the estimation of sub-seismic strain. *Geological Society Special Publication No. 99*, 11-26.

R. J. Knipe. (1997). Juxtaposition and Seal Diagrams to Help Analyze Fault Seals in Hydrocarbon Reservoirs. *AAPG Bulletin*, *81 (1997)*. https://doi.org/10.1306/522B42DF-1727-11D7-8645000102C1865D

Reynolds, A. D. (2017). Paralic reservoirs. *Geological Society, London, Special Publications*, *444*(1), 7–34. https://doi.org/10.1144/SP444.10

Snippe, J., Kampman, N., Bisdom, K., Tambach, T., March, R., Phillips, T., Inskip, N. F., Doster, F., & Busch, A. (n.d.). *Modelling of long-term along-fault flow of CO_2 from a natural reservoir*.

SLB. (2008, 01 01). *Schlumberger*. Retrieved from Schlumberger: https://www.slb.com/-/media/files/oilfield-review/the-prize-beneath-the-salt

Smith, S. (1988). *Tiger Shoal Field Offshore Louisiana.* New Orleans: AAPG.

Taylor, W. L., & Pollard, D. D. (2000). Estimation of in situ permeability of deformation bands in porous sandstone, Valley of Fire, Nevada. *Water Resources Research*, *36*(9), 2595–2606. https://doi.org/10.1029/2000WR900120

Timur, A. (1968). An investigation of permeability, porosity, & residual water saturation relationship for sandstone reservoirs. *The Log Analyst*, 9(04).

Treviño, R. H., Meckel, T. A., & Bureau of Economic Geology. (2017). *Geological CO_2 Sequestration Atlas of Miocene Strata, Offshore Texas State Waters* (Report of Investigations) [Report of Investigations]. The University of Texas at Austin, Bureau of Economic Geology. https://doi.org/10.23867/RI0283D

UN. (2015, 12 15). *The Paris Agreement*. Retrieved from United Nations: https://unfccc.int/process-and-meetings/the-paris-agreement

Urban S. Allan (2). (1989). Model for Hydrocarbon Migration and Entrapment Within Faulted Structures. *AAPG Bulletin*, *73*. https://doi.org/10.1306/44B4A271-170A-11D7-8645000102C1865D

Van Genuchten, M. Th. (1980). A Closed-form Equation for Predicting the Hydraulic Conductivity of Unsaturated Soils. *Soil Science Society of America Journal*, *44*(5), 892–898. https://doi.org/10.2136/sssaj1980.03615995004400050002x

Van Genuchten, M. (1980). A closed-form equation for predicting the hydraulic conductivity of unsaturated soils. *Soil Science Society of America Journal 44.5*, 892-898.

William E. Galloway,1 Patricia E. G. (2000). Cenozoic depositional history of the Gulf of Mexico basin. *AAPG Bulletin*, *84*. https://doi.org/10.1306/8626C37F-173B-11D7-8645000102C1865D

Yaghoubi, A. (2019). Hydraulic fracturing modeling using a discrete fracture network in the Barnett Shale. *International Journal of Rock Mechanics and Mining Sciences*, *119*, 98–108. https://doi.org/10.1016/j.ijrmms.2019.01.015

Yielding, G. (2002). Shale Gouge Ratio—Calibration by geohistory. In *Norwegian Petroleum Society Special Publications* (Vol. 11, pp. 1–15). Elsevier. https://doi.org/10.1016/S0928-8937(02)80003-

Zulqarnain, M. e. (2023). GCS site selection in saline Miocene formations in South Louisiana. *International Journal of Greenhouse Gas Control*, 13.